UNIVERSIDAD CARLOS III DE MADRID

Aerospace Engineering

TFG
Design and analysis of µPPT

Author:

Adrián Rubio García

Abstract

Cubesats constitute an inexpensive access to space and are one of the fastest growing technologies in the space industry. A micro pulsed plasma thruster (µPPT) is going to be modeled and designed in this paper to accomplish the requirements implied in cubesat dimensions and to perform drag compensation for an specific satellite mission. The performance of the thruster is going to be analyzed to fulfill, in the most effective way, the mission requirements.

Contents

List of Figures

List of Tables

1 Introduction

1.1 SmallSats socioeconomic framework

Over the duration of the last 20 years, Smallsats have evolved from something nearly inappreciable to a powerful and growing sector in the space industry. They are a low cost mean of reaching space, a launch of a single CubeSat costs roughly 80.000 $ and is usually done piggypacked in groups of around three SmallSats on launchers delivering larger spacecrafts in orbit. At the beginning its low cost and short development times make them very attractive as a test bed for new technologies, so only small research groups got involved in its maturation, over time industry such as The Aerospace Corporation and Boeing and national space agencies such as NASA and ESA realized the benefits and participated in the development of this type of satellites. The present researches reveal that about a third of the 2.500 satellites launched in the last 5 years had a wet mass (fuel included) below 500 kg, therefore called Smallsats, and the amount of them launched in the last 5 years is nearly equivalent to the accumulated amount of the 15 years before. A table with the definitions of the different types of Smallsats is included for clarification.

SmallSats	Wet Mass
PicoSatellite	$\leq$ 1 kg
NanoSatellite	1 - 10 kg
MicroSatellite	11 - 100 kg
MiniSatellite	101 - 500 kg

Table 1: Classification for SmallSats.

This strong trend of making satellites as small as possible is expressed in terms of units with the definition of the CubeSat Design Specification as Units (U) with a wet mass of m<1.33 kg and dimensions of 10 x 10 x 10 cm. Commonly-used Cubesats have form factors of around 1-6U.

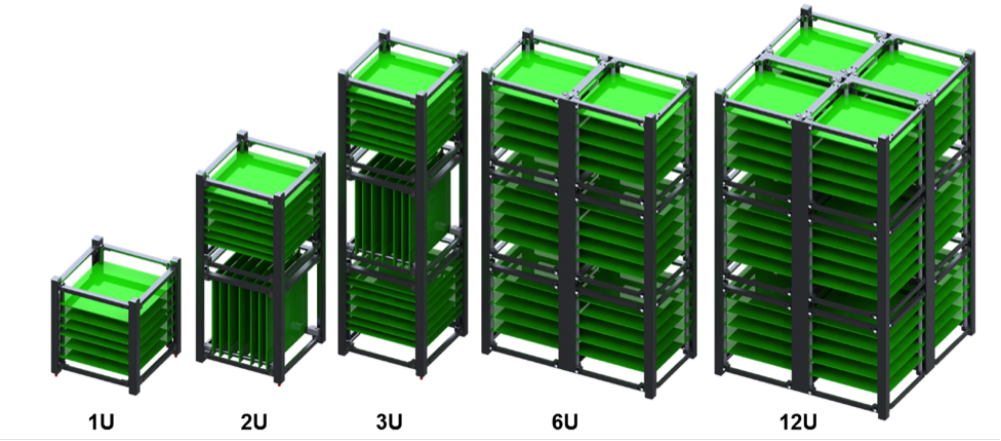

Figure 1: Cubesat Size comparison [6].

Once in orbit, CubeSats only need attitude control to achieve a life time of even 25 years, so propulsion means are strongly needed to fulfill this purpose in the most efficient manner.

1.2 Propulsion alternatives

In this section different propulsion means are going to be analyzed trying to find the choice that best fits in the specifications and constraints involved when dealing with SmallSats.

1.2.1 Solid propellant

Solid propellant devices are, of course, a chemical propulsion system quite versatile. With many sizes, they can provide from 2 N to about 12 MN. This range of thrust is much greater than the one looked for when talking about satellite control.

Additionally, this propulsion system has another huge inconvenience, they cannot be ”switched off”, once ignited they will burn until all the propellant gets consumed, and with little in-flight control over the thrust produced. Obviously for SmallSats operation multiple impulses are needed at different moments to maintain the satellite on its orbit.

Figure 2: Vega Launcher, project Ariane from ESA [32].

Nevertheless, solid propellant rockets are used as launchers (fig. 2), sounding rockets, missiles, etc. Applications in which its simplicity compared with liquid rockets and its giant thrust potential offer a non comparable performance.

1.2.2 Liquid propellant

Liquid propellant systems are another type of chemical propulsion. They offer about 50% higher specific impulse than the solid ones, and also higher thrust-to-weight ratio. For the purpose looked here, they ensure a control over the thrust by regulating the amount of propellant through the use of valves.

Of course, its main drawback lies in the complexity of their construction (valves, fuel tanks, pumps, etc.). This issue becomes a determinant factor when trying to fit a propulsion system in a 10 x 10 x 10 cm satellite. In addition, some of the liquid propellants are highly toxic (hydrazine) or cryogenic (liquid hydrogen), being difficult to work with.

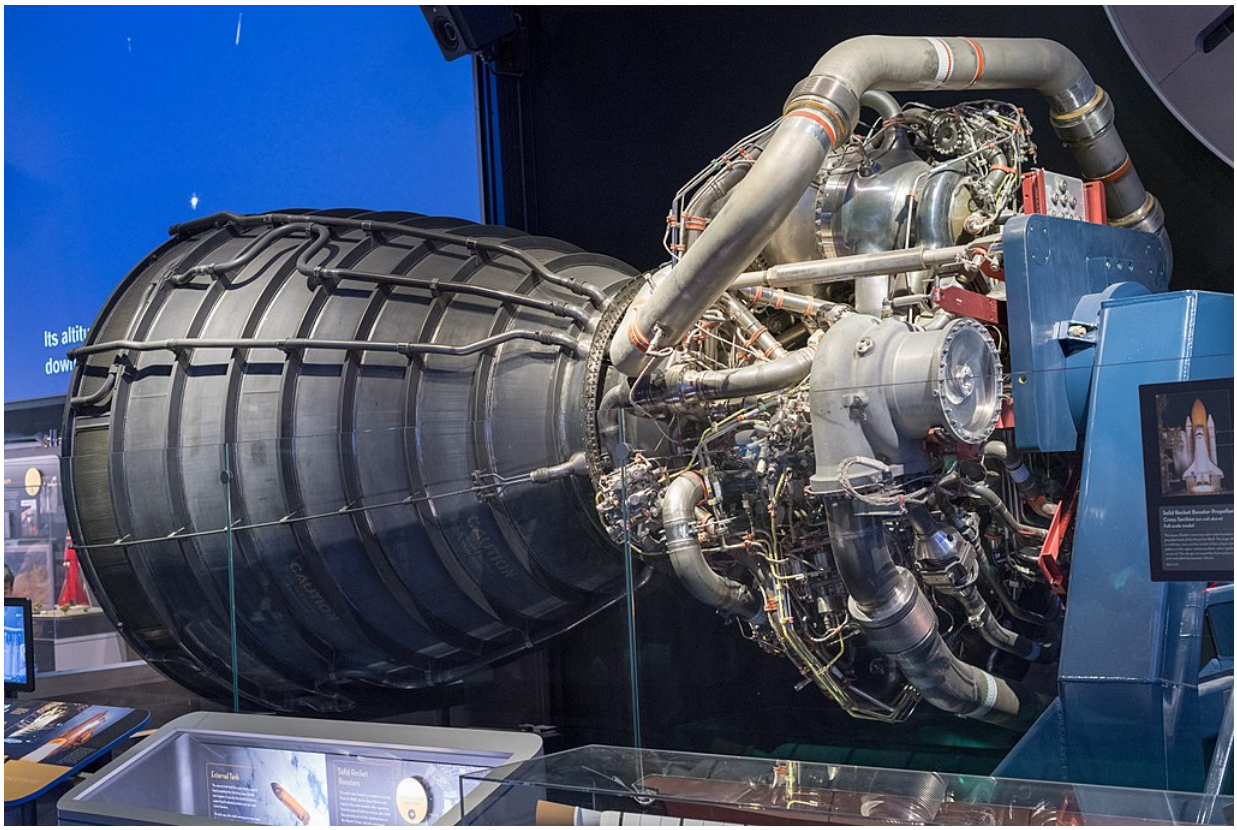

Figure 3: Aerojet Rocketdyne RS-25 [15].

Liquid propulsion devices are used also in launchers, one of the main examples of its great performance is the Aerojet Rocketdyne RS-25 (fig. 3), or best known as the Space Shuttle main engine (SSME). It is a liquid cryogenic rocket engine used on NASA's Space Shuttle, this engine is able to produce 1859 kN of thrust at liftoff and 366 s of specific impulse at sea level conditions. The Space Shuttle used a cluster of three RS-25 engines with additional thrust being provided by two solid rocket boosters.

1.2.3 Electric propulsion

The main advantage encountered when using electric propulsion is that the energy limitation is completely avoided, main roof when dealing with chemical propulsion. Electric propulsion is not energy limited, but power limited to the available power depending on the source used.

As simple as can be explained, in electric propulsion devices plasma gets formed by supplying enough energy to a low-pressure gas producing collisions between electrons that ionize neutral atoms. Plasma contains both free charges and neutrals, but is globally quasineutral, with the

exception of some particular places such as near the walls. These charges respond to electric and magnetic fields and gets accelerated due to its presence producing thrust.

Three main families in the electric propulsion world are distinguished:

1. **Electrothermal.**

   The Resistojet is the simpler of them all. A non-reacting gas is introduced into a small chamber with a resistor in its interior, this resistor heats up the gas to high temperatures and then the gas gets expanded through a nozzle to produce thrust. Its limitations lie in the maximum heating of the resistor and the maximum allowed wall material temperature. Its specific impulse is low, around 400-600 s, and can achieve thrusts up to 0,5 N.

   The Arcjet has a central cathode in its interior and its surrounded by an annular anode. A differencial in voltage is applied between them to generate an arc to ionize and heat the propellant. The key in this arrangement is that the center of the jet is what is most heated, reducing the wall-heating limitation that Resistojets have. It can achieve I_{sp} in the order of 1000 s.

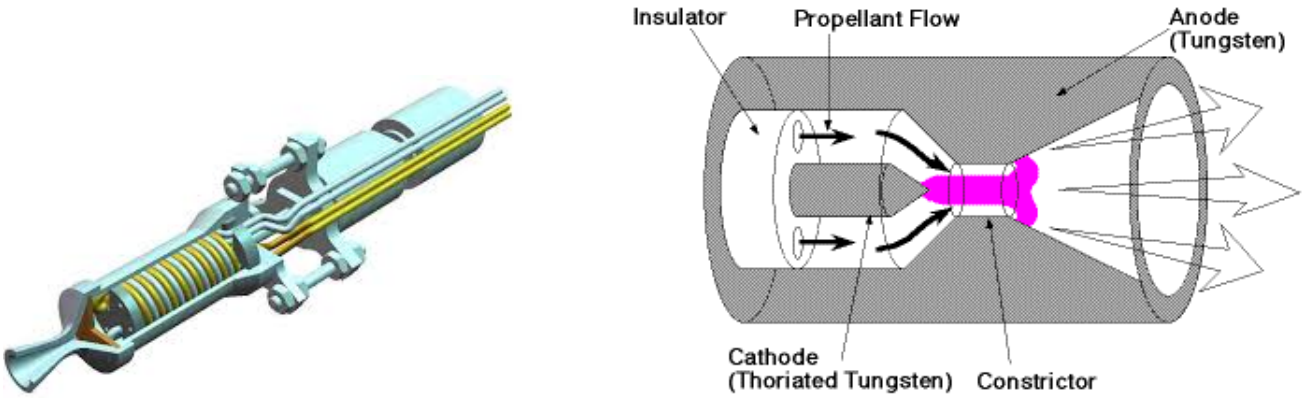

Figure 4: Resistojet [21] (left) and Arcjet [38] (right).

2. **Electrostatic.**

   In this type of thrusters, the propellant is broken down into ions and electrons (plasma) and an electric field is applied between two grids to accelerate ions to very high velocities. A neutralizer is key in these devices to avoid the charging of the electrons ejected.

   Gridded ion thrusters are one of the most successful electrostatic thrusters. They have an internal cathode emitting electrons, which collide with the neutral propellant creating

plasma. The ions enter the grids meanwhile electrons are repelled (through the application of an electric field), these region between grids is not anymore a quasineutral plasma. Then this same electric field is capable of accelerating the ions and with the help of an external cathode, called neutralizer, the flow comes back to a quasineutral state again. The presence of a internal magnetic field make the electrons gyrate increasing its ionization rate and the thruster performance. Having an specific impulsed around 2000-10000 s, these are the highest I_{sp} achieved nowadays.

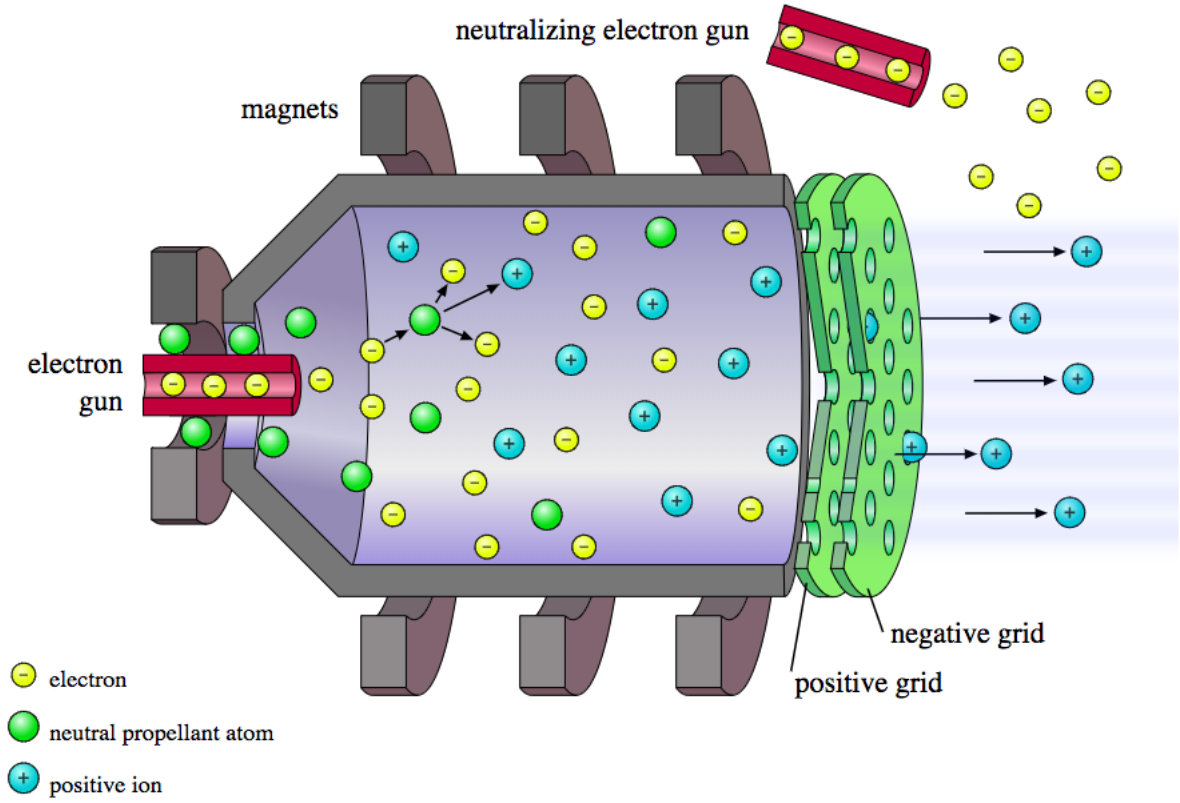

Figure 5: Gridded ion thruster.

3. **Electromagnetic.**

In EM thrusters the need of grids is avoided using simultaneously electric and magnetic fields to accelerate quasineutral plasma.

Hall effect thrusters consist on an annular cavity chamber in which the anode is located in the rear wall and the cathode is placed outside. This cathode emits electrons towards the anode that hit and ionize the neutral gas creating a plasma. A radial magnetic field is applied in the channel causing the electrons to gyrate and drift in the azimuthal direction

increasing its residence time through the chamber about a hundred times. These electrons, unable to short-circuit the discharge due to the presence of the magnetic field, are accelerated outwards again by the electric field. Notice that in these devices the cathode acts also as a neutralizer since some of the electrons flow downstream to achieve a quasineutral plasma. They offer a great specific impulse (1000-2000 s) at a great range of powers (0.5-15 kW), having an efficiency $\mu_T \approx 50\%$. Their main drawback lies in a limited lifetime of less than 10000 h.

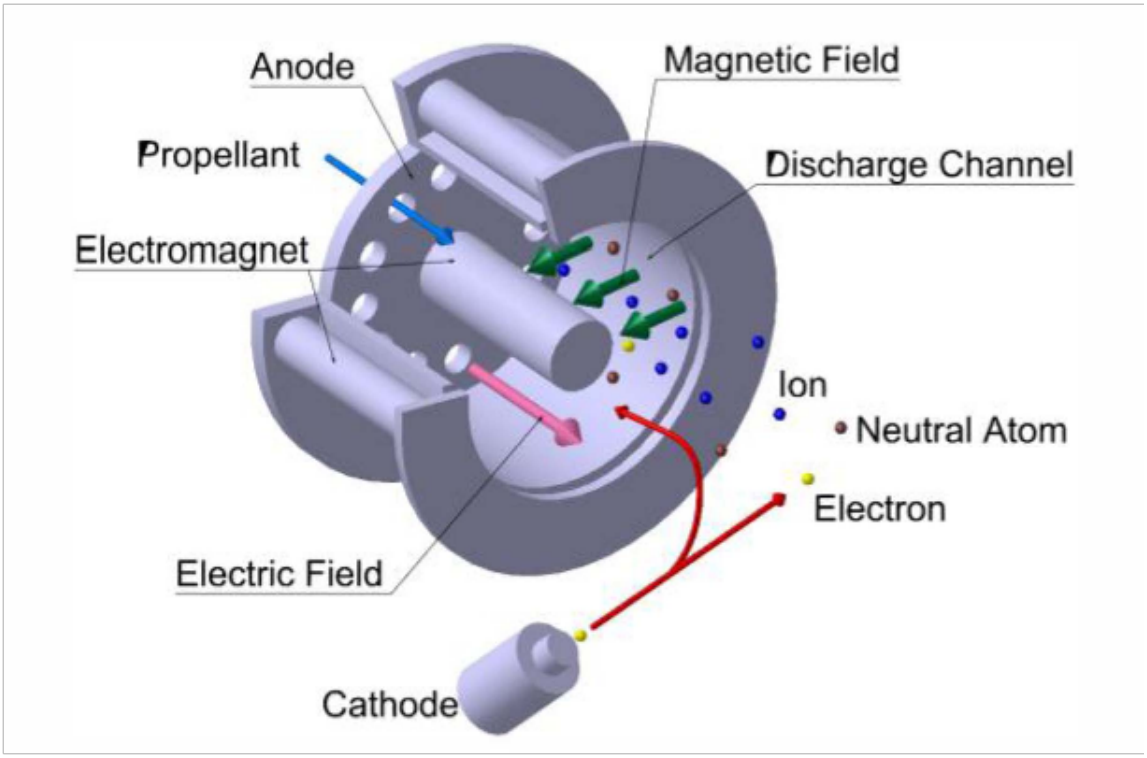

Figure 6: Hall effect thruster [22].

Pulsed plasma thrusters (PPTs) take advantage of a fast discharge between two plates (cathode and anode) to generate a high electric current that vaporizes and ionizes a thin layer of propellant, usually teflon. The now closed current loop creates a magnetic field, and due to the interaction between the electric and magnetic field a Lorentz force appears accelerating the plasma through the channel. Its efficiency and specific impulse are modest: $\mu_T \approx 10\%$, $I_{sp} \approx 1000$. Its difference and huge advantage from other electrical propulsion thrusters lies in the simplicity of its design and construction, roughly a spring to maintain the teflon in place and a capacitor to initiate the discharge, and in the very precise control in thrust

obtained through the alteration of the pulsed frequency. PPTs have already been proven as a successful solution at orbit and attitude correction, together with its great scalability to be implemented in SmallSats due to its simpleness, make PPTs the topic of this paper.

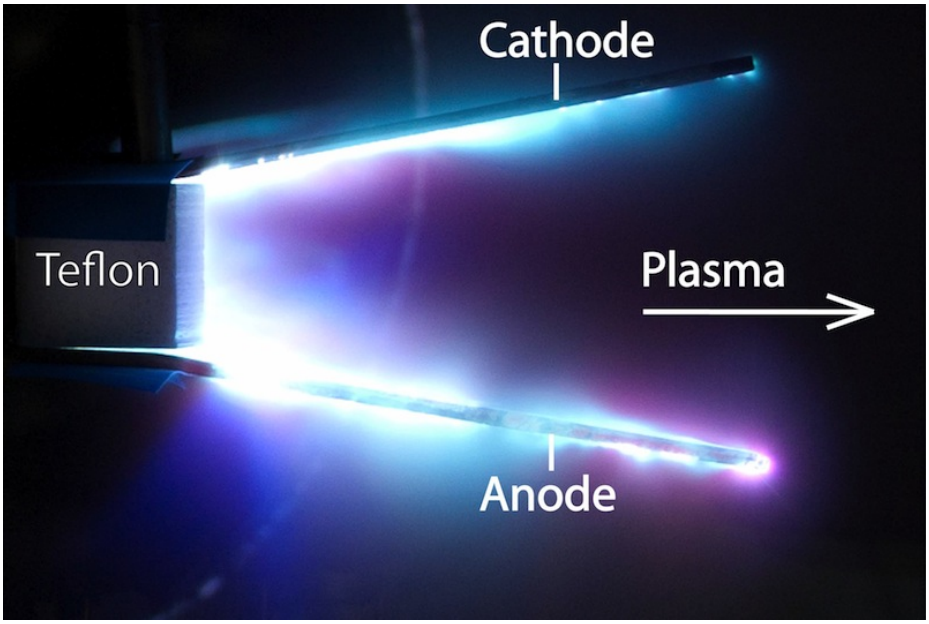

Figure 7: Pulsed plasma thruster [34] (PPT).

Figure (8) has been included to summarize the performance domain of the different types of electric propulsion devices. Notice that PPTs lies at the bottom of the graph, demanding the lowest values of power of them all, but providing a reasonably high results of specific impulse. For this same reason they constitute an smart solution for the cubesat propulsion problem.

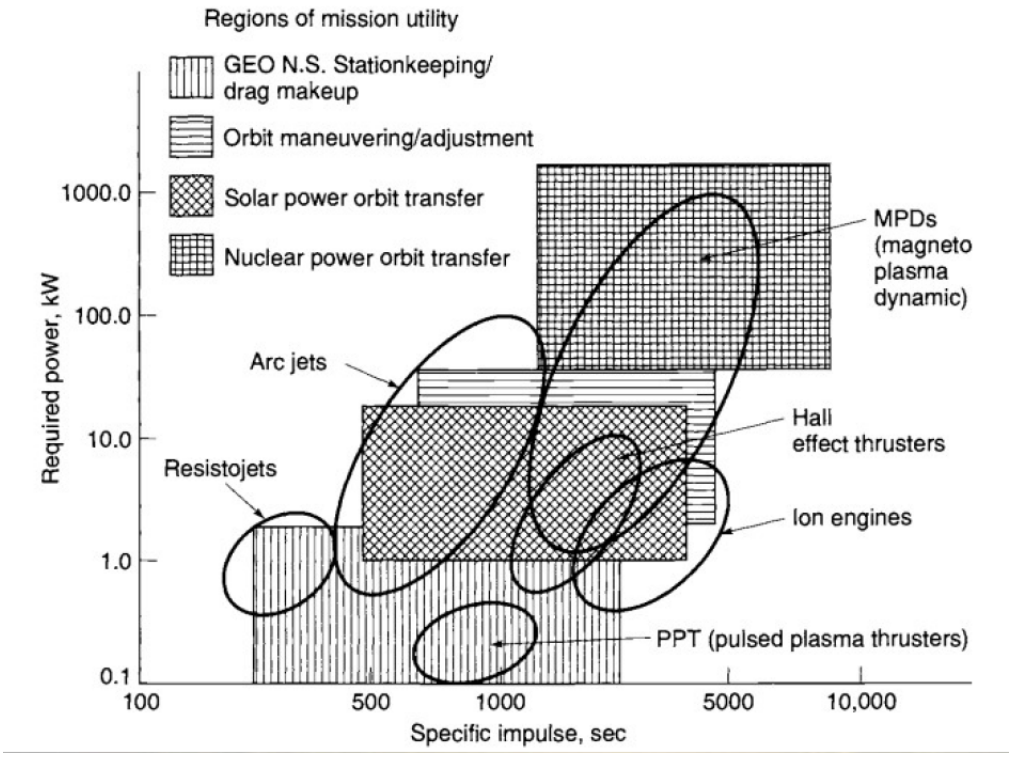

Figure 8: Operational domain for different electrical propulsion devices.

1.3 Basic principles of PPT

First thoughts of pulsed plasma acceleration can be inferred from phenomenological observation, its basic process can be understood with some laboratory devices. Considering a pair of parallel electrodes, as sketched in fig.(9a). Having a large capacitor charged with a sufficiently high initial voltage, when abruptly switched across these rails, an arc will form between them at the leftmost position and will propagate down the rails. This effect can be observed too in a botton gun, fig.(9b), where the plasma created is normally ejected outwards; in a T tube, fig.(9c), where plasma discharged impels a shock wave down a glass pipe; in a coaxial gun fig.(9d), where an annular sheet of plasma sweep between coaxial conductors; and in a dynamical pinch, fig.(9e), where a cylindrical plasma sheet this time implodes inward from the electrode periphery.

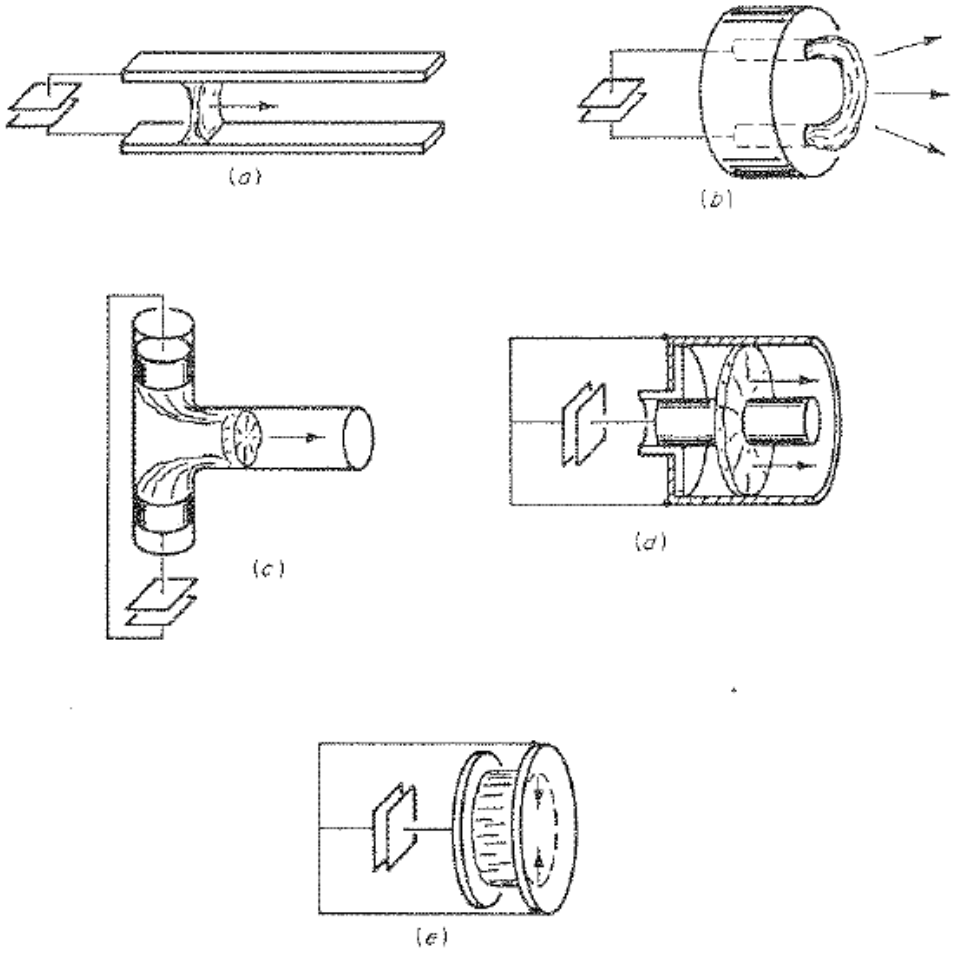

Figure 9: Pulsed plasma accelerators [30]. a) Parallel-rail accelerator; b) Botton gun; c) T tube; d) coaxial gun; e) linear pinch.

The physics underneath this phenomena can be understood thanks to Hendrik Antoon Lorentz, a Dutch physicist known for the Lorentz force among other influential studies. The Lorentz force is better understood with the help of figure (10), in which it is observed that, when the discharge occurs, the current loop gets closed inducing a perpendicular (into the paper in the example) magnetic field. Then, the Lorentz force appears perpendicular to the plane formed by the electric and magnetic fields, following of course the right-hand rule. It is important to notice that, independently of the direction of the current, the force will always point outwards the channel, as both electric and magnetic directions would be opposite to the presented in fig.(10).

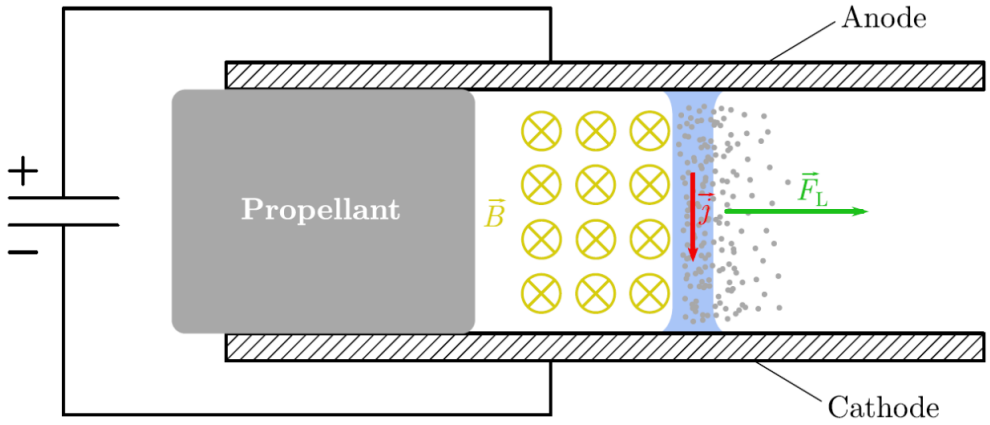

Figure 10: Lorentz force visualization.

1.4 History and state of the art of PPTs

The Pulsed Plasma Thruster (PPT) was the first electric propulsion device ever put in space, it was on the Soviet Zond-2 mission. Since then, they have been employed in diverse space utilizations varying from drag compensation (TIP/NOVA with a total of 28 thrusters) to east-west station keeping (LES-6) and attitude control (SMS and LES-8/9).

The mechanical simplicity coming from the use of a solid propellant and from the avoidance of a neutralizer, the relatively high specific impulse at low levels of power and its successful historical background as a space tested electrical propulsion solution, make PPTs an ideal candidate for CubeSats.

Due to the above, the Fotec team, comissioned in 2006 by the Austrian Space Agency, started to develop a miniaturized Pulsed Plasma Thruster (µPPT). Initially the efforts were put in the establishment of a numerical tool aimed to support the understanding of the effect that this scaling could have on the parameters and properties of the circuit elements, these efforts resulted in a one dimensional electromechanical model well experimentally verified. This model were the key to investigate different design variations included standard parallel plate PPT with varying discharge channel geometries and electrode designs, later on tongued and flared electrodes and variations of electrode materials and electrode thickness were also considered.

Nevertheless, even having a useful model that corresponds with the experimental results, persistent lifetime problems mainly linked to the ignition system arose. No commercial ignition system

enough miniaturized and with suitable lifetime were available. Therefore, the focus shifted to a coaxial µPPT, fig.(11), the subsequent developments focused on the design of the main discharge electrodes and on the nature of the ignition electrode (geometry, location, etc.) made clear that this symmetric rotational design is by far superior to the parallel plate one in terms of reliability and lifetime, achieving more than 600.000 discharges (compared with around 70.000 for the parallel plate system).

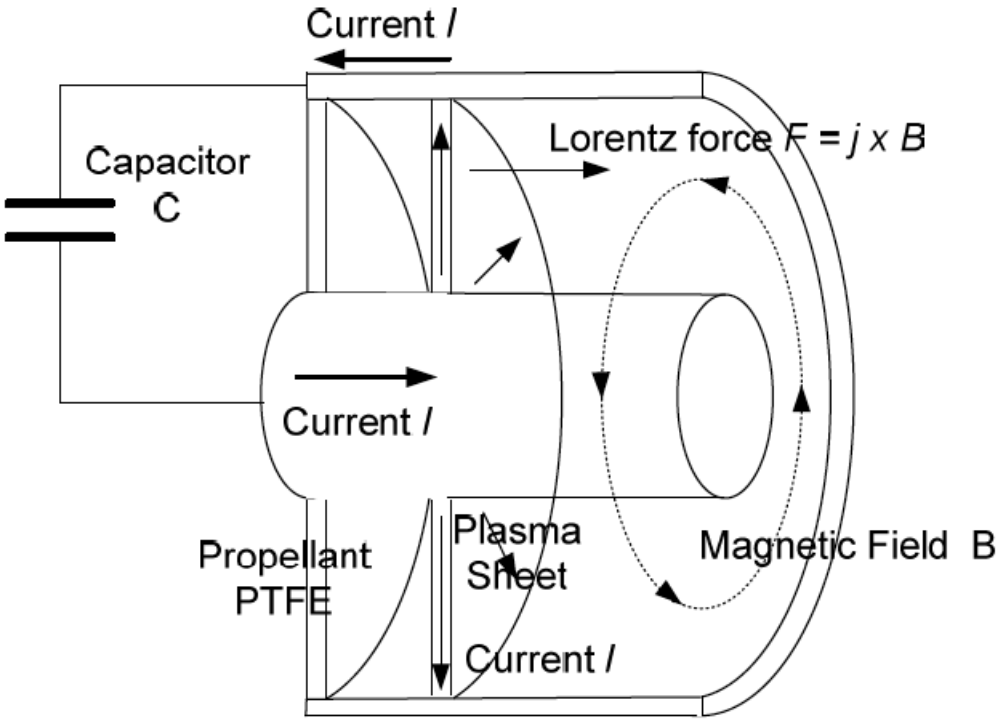

Figure 11: Coaxial PPT representation [4].

Nowadays, Clyde Space and Mars Space Ltd. [2, 3] have developed a Teflon PPT for cubesats capable of 650 s I_s with up to 45 µN-s of impulse bit, fig.(12). Fotec [4] has also developed another PTFE (Teflon) PPT module with 900 s of specific impulse and impulse bits from 3.5-10 µN-s. Busek Company Inc. [5] has also two different systems available that operate on PTFE µPPT, one with 3 thrusters and one with 9 thrusters, both configurations with flight heritage on FalconSat-3 are designed to provide active attitude control.

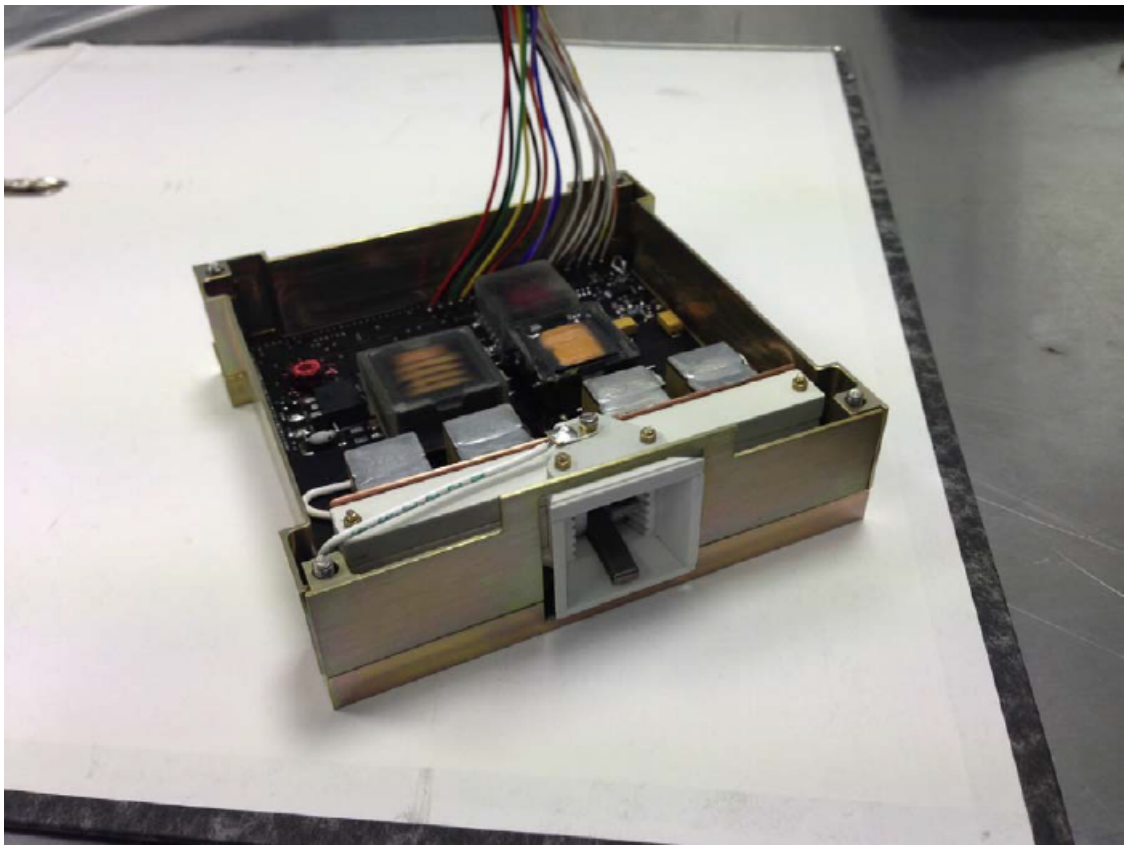

Figure 12: µPPT developed by Clyde Space and Mars Space Ltd. [7].

Liquid PPTs have been growing recently for cubesats. They offer the performance versatility obtained by varying the amount of propellant ejected per pulse, but in exchange they require more complex feed systems when compared with solid PPTs. A Liquid Micro Pulsed Plasma Thruster (LµPPT) developed by QuinteScience and the Institute on Physiscs and Laser Microfusion [7] in Poland operates in a non-hazardous liquid propellant (perfluorpolyether) producing specific impulse ranging from 1000-1400 s with impulse bits of 10-25 mN-s.

1.5 Outline

In this paper, the physical concept that lies beneath this type of electric propulsion will be perfectly understood in detail. Some models are gonna be presented to make an estimation of the main parameters needed to put this device on track and also an analysis of its performance will be crucial to have an idea of how this PPTs fit in the requirements demanded for a SmallSat (efficiency, thrust, etc.). Finally, a preliminary design to accomplish certain mission requirements for the drag compensation of a 3U cubesat is going to be exposed, with the objective of bringing to life

this design at Universidad Carlos III de Madrid and enable the possibility to prove the validity of the models and conclusions in this paper through the comparison with experimental results.

2 Modelling

2.1 Physical concept

PPTs provide thrust through a series of impulse bits, this main difference with other types of steady electric propulsion presents three potential advantages:

1. The thrust efficiency tends to improve with increasing discharge current density. In this type of space thruster this maximum current will be limited either by the available power supply or by the electrode erosion, so there would exist some advantage in passing this current intermittently obtaining a higher average thrust with, probably, less electrode erosion.

2. Operating with intense pulses may vanish the development of undesirable kinetic phenomena within the accelerating plasma. For example, with a rapidly enough acceleration, the free-electron component of the gas could avoid thermalizing in contact with the ions, and subsequently not wasting this energy via inelastic collisions and radiation.

3. Unsteady electromagnetic field may produce beneficial nonuniformities through the channel. The most known example is the ”skin effect”, where the entire current may be constrained to flow in a narrow region in the discharge channel, thereby providing a more effective between the accelerating field and the ambient gas.

Taking a look at the schematic representation of a parallel-plate PPT (fig. 13) it can be understood the basics of the phenomena occurring through this electro-dynamic thruster. Once the switch is on a charged capacitor discharges between two electrodes, the arc resulting from this discharge produces the ablation of the propellant with the help of the ignition plug (in the case of solid propellant). The acceleration itself is mainly produced due to the interaction between the arc current and the self-magnetic field produced by the complete closed circuit. No matter the sign of this current, the magnetic field induced produces always a force trying to expand this closed loop, and therefore driving the plasma away from the channel formed by the electrodes.

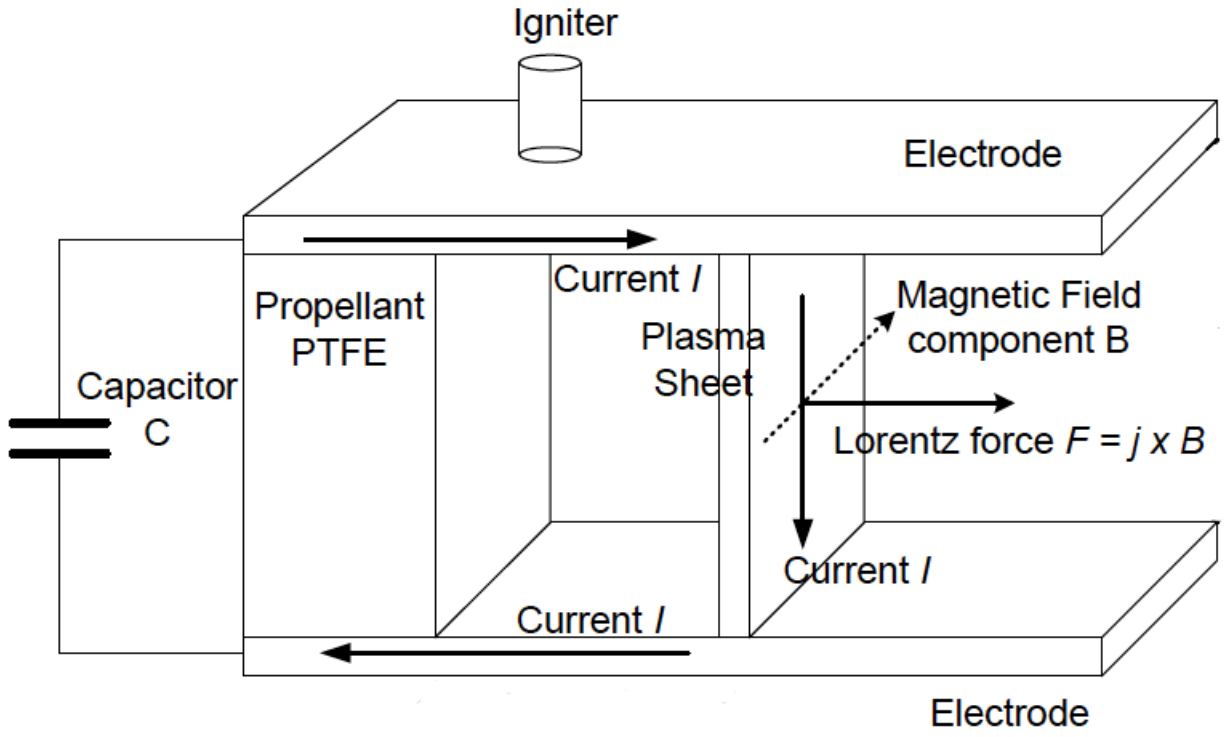

Figure 13: Schematic representation of a PPT.

To achieve the correct functioning of this type of device, it must properly fulfill a sequence of gasdynamic processes that starts from the initial filling of the gap with propellant gas (in case of solid, ablation), a correct channeling of the plasma through the acceleration phase, and the ejection of the accelerated mass at the end of the channel. This cycle can be better understood splitting it in the following series of events:

1. Firstly, the necessary amount of electrical energy must be accumulated in the external circuit. Seeking for pulses with very large current (10^4 to 10^6 amp), and at enough voltage to break down a few centimeters of cold gas (10^3 to 10^5 volts), a capacitor will be required. When switched this storage unit must deliver its electrical energy dissipating as minimum as possible.

2. Then, the propellant gas has to be introduced in the electrode gap generating the desired mass density distribution prior to discharge. In its normal life, the exit opens directly onto free space, hence, gas injection must be accomplished quick enough and in accurate correlation with the discharge initiation. It is not desired to leak out too much gas before

breakdown or release the gas once the event is over. Meanwhile for a single pulse or relatively slow repetitive operation an extremely rapid valve, for very high frequency operation may be of interest to implement a steady inlet flow.

3. Discharge breakdown, as commented, has to be precise in time but also in space, it must occur at the proper geometrical location in the channel. This is normally relatively easy due to the aforementioned "skin effect". The timing problem can be faced either with a switch in the external circuit or a precise combination of the breakdown potential against the pressure characteristics of the propellant. The use of an external switch allows correct correlation between the discharge and the gas-filling, but in exchange will inevitably consume some energy adding also some inductance to the circuit. On the other hand, self-triggering of the discharge eliminates the switch, but it restricts the operation of the PPT to a particular combinations of gap spacing, applied voltage and gas density, limiting its versatility as well as provoking significant dissipation at the breakdown phase.

4. Discharge fulfilled, it must be accomplished rapidly a stable current layer that covers the entire cross section of the channel and with sufficiently high conductivity to make resistive losses negligible, this means a sufficiently dense layer to be impermeable to the ambient gas and in this way achieve its acceleration. These requirements depend, first, on the external circuit, which must be able to provide sufficient total current at rapid rise time; second, on the ambient gas density, it must be high enough to sustain the arc but not overload it with excessive mass; and third, on the channel geometry, which must accommodate the cross section current zone through the entire length.

5. Now that the current layer is formed, it must be accelerated down the channel under the influence of its own magnetic field, accumulating effectively the ambient gas either by pushing it or by entraining it within the layer itself, until the desired velocity is reached. It is important that during this process the current layer does not become porous allowing the gas ahead to flow through it, nor develop dynamic instabilities that could disrupt its profile. In addition, this gas accumulation process should include also a minimum thermalization and dissipation in the current layer.

6. Once the accelerated gas and plasma reaches the end of the channel, at the time of the ejection the thermal and electromagnetic losses have to be minimized. On one hand, the

magnetic field prevailing near the exhaust may contribute to focus the plume into a well-collimated stream inducing, hence, a correct recovery of thermal energy. On the other hand, this field must not impede plasma's ejection in a dynamical sense, plasma should not become tied to the field lines. Finally, the reminiscence of electromagnetic energy must not be large enough to relapse into the external circuit, producing dissipation in useless secondary breakdowns.

7. At the very end, the system must return to its initial situation, before a new cycle starts again. It could seem the simplest part but in here are involved several processes, such as the recharging of the capacitor, the relaxation of residual ionization left in the channel, the completion of the gas valve cycle, the rearming of the switch, etc. The smallest error in any of these could infer a deterioration in the performance of the PPT through the cycles.

It is important to notice that in solid propellant PPTs the ablation of the propellant to transform it into gas is a complex process, objective of numerous studies.

The sum of all of this requirements constitute an intricate mechanism that, minding every single detail of it, offers an efficient conversion of electrical energy into kinetic energy at the exhaust. In here, analytical models play a crucial role to try to accomplish all the specifications and, in this way, fully understand the performance of PPTs, these models will be now studied meticulously.

2.2 Circuit analysis

The physical concept of narrow current layers in accelerators like these suggests an analytical idealization where these layers are represented by discrete movable elements of a inductance-capacitance-resistance (LCR) series circuit. Taking a glance at fig.(14) this can be better understood, a capacitance C initially charged to a voltage V_0 is switched. Breakdown of the gas closes a circuit having already a certain initial inductance L_0, due to the proper geometry of the circuit and the inherent inductance of the capacitors, and an initial resistance R_0, partly by the external circuit and by the discharge itself. This idealization forms the circuit configuration shown at the lower right part of fig.(14).

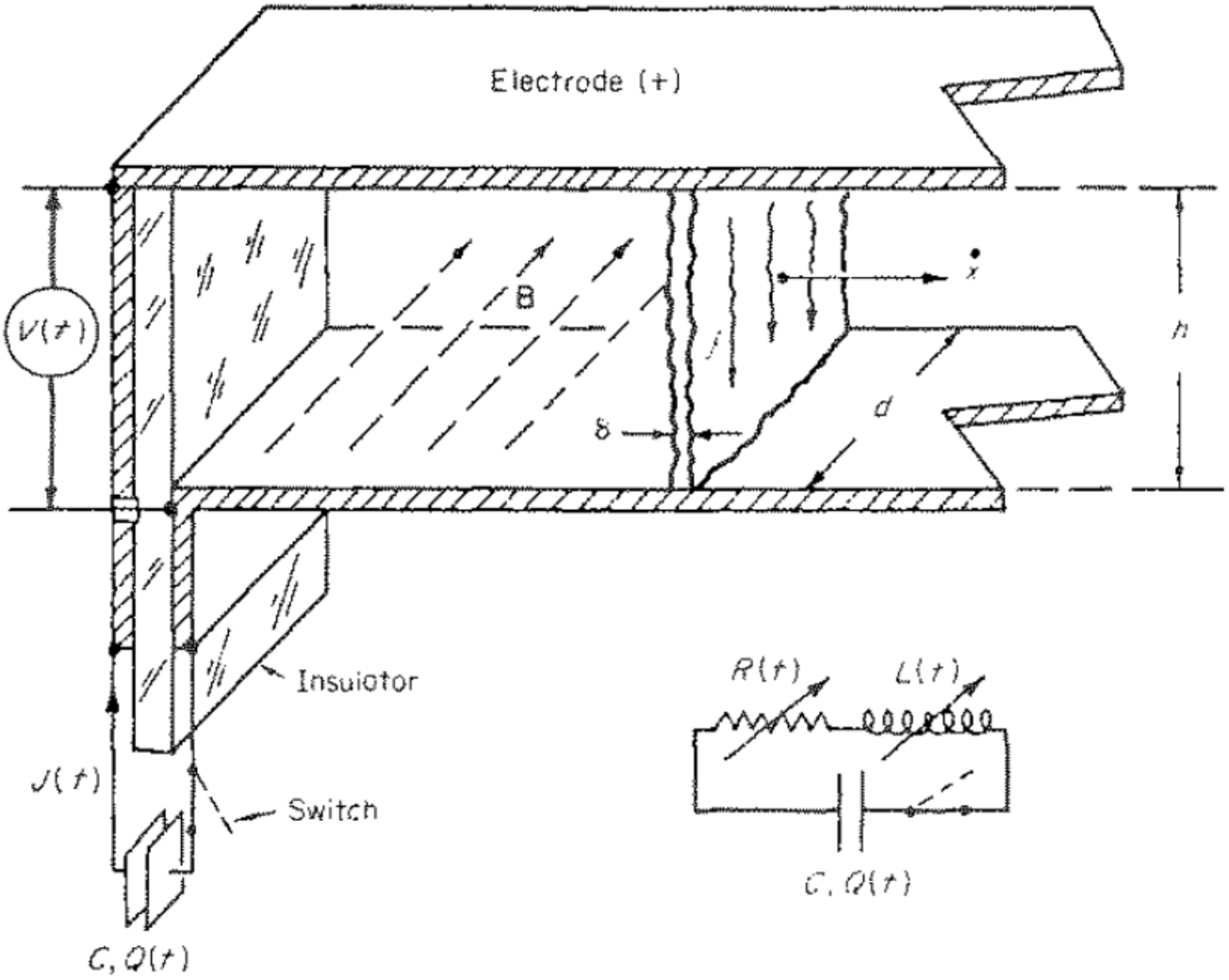

Figure 14: Parallel-plate circuit idealization [30].

Of course, as the discharge intensifies and the layer propagates down the channel, the inductance $L(t)$ will increase and the resistance $R(t)$ will change as well in time, both in response of the waveforms of current flowing through the circuit $J(t)$ and voltage alterations across the electrodes $V(t)$. Application of Maxwell's equation $\nabla \times E$ yields the following

$$V = JR + \dot{\phi} = JR + \frac{d}{dt}(LJ) = JR + L\dot{J} + \dot{L}J \tag{1}$$

where there exist two contributions to the voltage, JR coming from the resistance, and the rate of change of ϕ coming from the capacitor, being ϕ the magnetic flux defining the inductance L. The power delivered by the capacitance is simply the current times the voltage,

$$P = JV = J^2R + LJ\dot{J} + J^2\dot{L} = J^2R + \frac{d}{dt}\left(1/2LJ^2\right) + 1/2J^2\dot{L} \tag{2}$$

the disposal in the three terms presented at the rightmost of eq.(2) is not arbitrary, they represent, respectively, rate of resistive heat generation, rate of change of energy stored in magnetic fields, and finally, the desired term to be optimized, the rate of work done on the moving arc sheet.

Considering the energy initially stored in the capacitance as $W_0 = 1/2CV_0{}^2$, that is delivered to the circuit in a time τ. We can write

$$W_0 = \int_0^\tau P dt = \int_0^\tau \left(J^2R + 1/2J^2\dot{L}\right) dt \tag{3}$$

where the energy term $\frac{d}{dt}\left(1/2LJ^2\right)$ had disappeared since the current is zero at $t = 0$ and $t = \tau$. Note that in this equation $\dot{L}$ has same dimensions as a real impedance (R). With these two possible outcomes of the initial energy stored by the capacitance one can easily define an electrical efficiency

$$\eta_e = \frac{1}{2}\frac{\int_0^\tau J^2\dot{L}dt}{W_0} \tag{4}$$

which assumes the J^2R integral as a total loss and the $J^2\dot{L}$ one as the part of the energy completely convertible to kinetic energy.

A simple, but useful, estimation of the magnitude of η_e can be performed. Defining a fictitious reference current J_0 equal to the amplitude of the sinusoidal current needed in this circuit to make R equal to zero and to establish a constant inductance equal to its initial value L_0, then eq.(3) yields $W_0 = 1/2L_0{J_0}^2$. As in the real circuit the impedance monotonically increases from L_0 and R is finite, it can be stated that $J < J_0$ throughout the pulse, and therefore eq.(4) gets transformed into the following inequality

$$\eta_e = \frac{\int_0^\tau J^2\dot{L}dt}{{J_0}^2L_0} < \frac{\int_0^\tau {J_0}^2\dot{L}dt}{{J_0}^2L_0} = \frac{\Delta L}{L_0} \tag{5}$$

where ΔL is the total increase in inductance achieved during a single current pulse. At a first

glance, this relation indicates that efficient single pulse accelerators will be determined mainly by the inductance change compared with its initial value. This criteria fails either because of excessive resistive losses or because of an uncoupling of the plasma layer from the circuit before completion of the pulse, therefore leaving behind energy residues in the capacitance and in the electromagnetic field.

This criterion gets related to the geometry and scale of the accelerator easily, and can be better understood by an order of magnitude examination. First, the plates of our PPT are desired to be sufficiently broad to avoid edge effects as much as possible, $h/d \approx 0.1$, the change of inductance they contribute is simply $\mu_0(h/d)x$, being x the displacement of the current sheet. And since the latter is the only time depending variable,

$$\dot{L} = \mu_0 \frac{h}{d} \dot{x} \tag{6}$$

Considering an exhaust speed $\dot{x} \approx 5 \times 10^4$ m/sec, $\dot{L}$ will not exceed about 0.005 ohm. Consequently, all resistances in the circuit must be small compared with this value as dissipation of the applied power in Joule heating is not desired. The change in inductance is very small too, even allowing the channel to be 0.5 m long, a generous size, ΔL would be about 5×10^{-8} henry, assemble a circuit with fixed inductance less than this value is a very delicate effort.

The required capacitance C and initial voltage V_0 are dominated by a number of conflicting factors, mainly by the current sheet opacity, by the ringdown pattern of the complete circuit, and by the specific mass of the capacitors. Empirically, it has been found that the minimum linear current density needed for the current sheet to accelerate and sweep ambient gas is around 10^5 amp/m; hence about 10^4 amp are required for a 0.1 m length accelerator (l). Therefore, $\tau = l/\dot{x} \approx 10^-5$ sec, the initial charge storage to sustain the pulse is $Q_0 \approx J\tau > 0.1$ coulomb and the capacitance $C = Q_0/V_0 > 0.1/V_0$ farad. The initial voltage is bounded from both up and down so it is large enough to accomplish the breakdown and drive the current sheet, but not so large to cause trouble from an insulation or power supply perspective, in this example $1000 < V < 20000$ volts, yielding a value for the capacitance from 5 to 100 µf.

The capacitance has a second constraint in relation to the LCR circuit, coming back to eq.1 it can be written as a differential equation in Q by stating $J = -\dot{Q}$ and $V = Q/C$:

$$L_0\ddot{Q} + R_0\dot{Q} + \frac{Q}{C} = 0 \tag{7}$$

This, considering as initial conditions $Q = Q_0$, $J_0 = -\dot{Q}(0)$ at $t = 0$, results in three different solutions:

1. For $C < 4L_0/{R_0}^2$ there is a damped oscillatory behavior.

$$\begin{aligned} Q &= \frac{Q_0}{w\sqrt{L_0 C}} e^{[-(R_0/2L_0)t]} \sin(wt + \delta) \\ J &= -\dot{Q} = \frac{Q_0}{wL_0 C} e^{[-(R/2L_0)t]} \sin wt \\ \textit{where} \quad w &= \left(\frac{1}{L_0 C} - \frac{{R_0}^2}{4{L_0}^2}\right)^{1/2} \\ \textit{and} \quad \delta &= \tan^{-1}\left(\frac{4L_0}{{R_0}^2 C} - 1\right)^{1/2} \end{aligned} \tag{8}$$

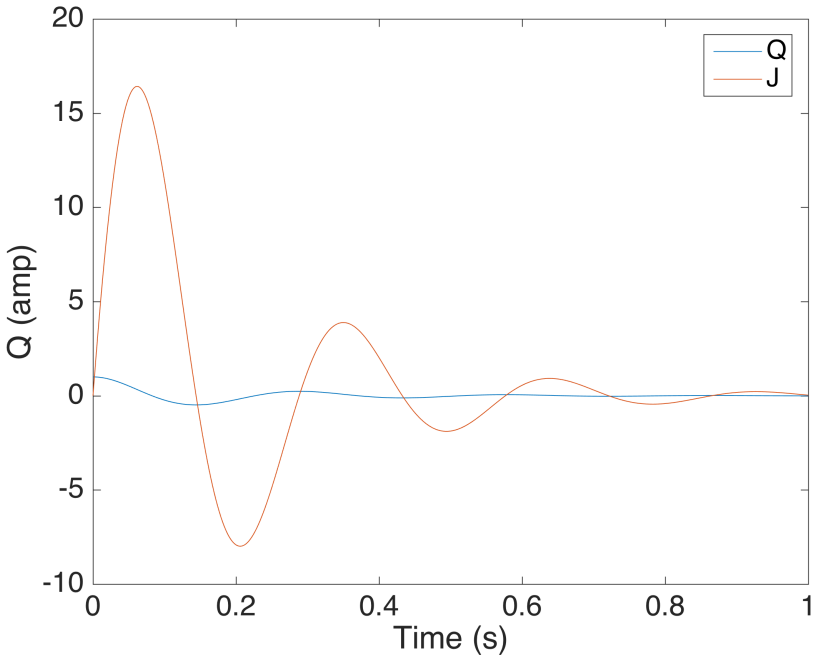

Figure 15: Underdamped LCR circuit

2. Having $C > 4L_0/{R_0}^2$ the current is overdamped.

$$Q = \frac{Q_0}{w'\sqrt{L_0 C}} e^{[-(R_0/2L_0)t]} \sinh\left(w't + \delta'\right)$$

$$J = \frac{Q_0}{w' L_0 C} e^{[-(R/2L_0)t]} \sinh w't \tag{9}$$

$$\textit{where} \qquad w' = \left(\frac{{R_0}^2}{4{L_0}^2} - \frac{1}{L_0 C}\right)^{1/2} = iw$$

$$\textit{and} \qquad \delta' = \tanh^{-1}\left(1 - \frac{4L_0}{{R_0}^2 C}\right)^{1/2}$$

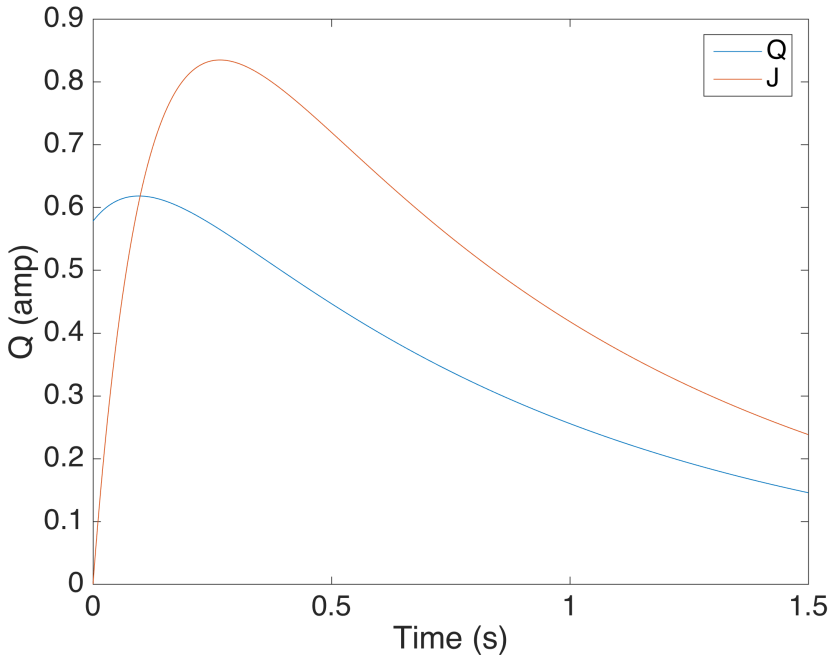

Figure 16: Overdamped LCR circuit

3. One last special case points out the situation at which the circuit is critically damped, $C = 4L_0/{R_0}^2$.

$$Q = Q_0 \left(1 + \frac{R_0}{2L_0} t\right) e^{[-(R/2L_0)t]}$$
$$J = \frac{Q_0}{L_0 C} t e^{[-(R/2L_0)t]} \tag{10}$$

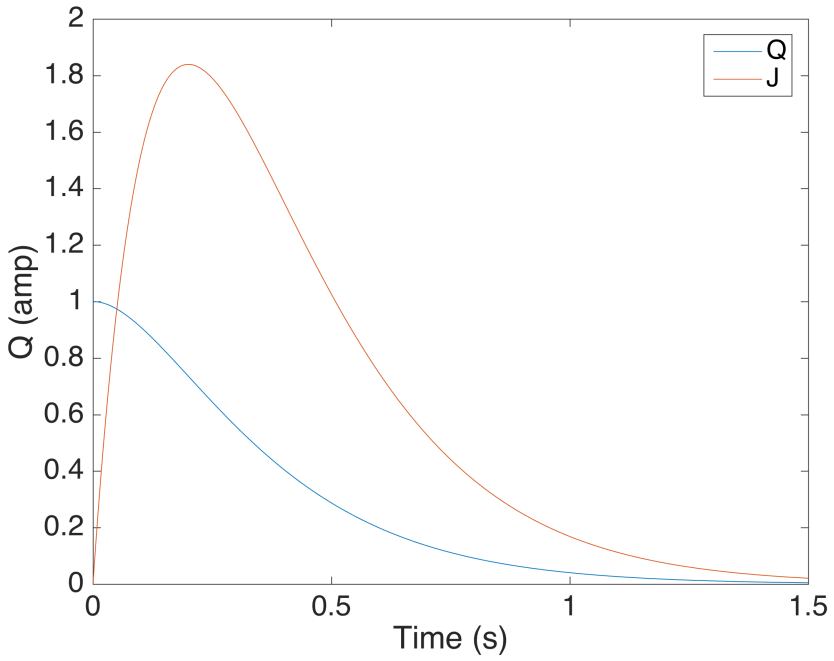

Figure 17: Critically damped LCR circuit

In the example above around 10^4 µf of capacitance would be enough to reach critical damping conditions. Nevertheless, this analysis from an electric point of view points out a value for the capacitance not compatible for our dynamic circuit both by the total mass and volume that would imply assembling such a capacitor and by the intolerable slow current rise time that goes with it. A 1 percent of this value is what is most probable to encounter at best, therefore the common situation is an underdamped circuit.

Using the minimum value of capacitance state before, say 5 µf, the period of oscillation ($T = 2\pi\sqrt{L_0 C}$) is shorter than the acceleration time, hence current reversals will take place while the plasma is going through the channel. In practice, it is observed that this current will not reverse to the initial current layer, but a secondary breakdown will occur at the initial position moments before the first discharge. Although these secondary discharges may also propagate down the channel, usually they are less controlled than the primary layer, as they only have upfront the residue of gas left behind by the primary sheet to take form and accelerate.

One can consider then the addition of capacitance until some extent of the period in which the acceleration time of the channel gets exceeded, and in this way avoid secondary breakdowns. However, this practice would reduce the current rise time to nearly one half the total pulse length, reducing the beneficial ”skin effect” and its effectivity to sweep the incoming gas. The better

approach to eliminate oscillatory trends in the circuit, without a huge capacitance and with no slow rise time, is with the assistance of a more complex configuration which could deliver a tailored pulse of current to our circuit.

The foregoing models to be studied help to achieve an intrinsic knowledge about the performance of this type of accelerator through the nearest approximation of the gas-sweeping process. The essential function of PPTs, as commented, is to accelerate mass by the magnetic forces, since the discharge current is itself determined by the position and velocity of the layer, this dynamical problem is nonlinear. More specifically, the microscopic details of the ionization of the ambient gas and acceleration of the current sheet are complex and obscure. Therefore, the usual approach to this kind of problem is an analytical one based on several models which represent, some better than others, the gross dynamical performance.

2.3 Slug model

It is the simplest idealization, the entire mass of gas to be accelerated is presumed to be enveloped in the initial breakdown at the minimum inductance, which means that since that time, no mass is accumulated or lost, mass is constant. The slug model is not adequate for most of the situations, but it provides a first glance into the scaling properties of PPTs.

Returning to the parallel-plate geometry represented in fig.(14) a thin layer of the sheet is considered having mass m/d, through this layer a current j is passing such as $j = \frac{J}{\delta d}$ and the magnetic field derived from the Maxwell equation is $\nabla \wedge B = \mu_0 j$ which yields

$$\frac{\partial B_x}{\partial z} - \frac{\partial B_z}{\partial x} = B_{zout} - B_{zin} = -\mu_0 \int_0^\delta j dx \Rightarrow \mu_0 \int_0^\delta j dx \tag{11}$$

.

Notice that the value of the magnetic field outside the current loop is equal to zero as it is assumed a quasi-infinite geometry. Newton's second law states

$$\frac{m}{d}\ddot{x} = h\int_0^\delta jBdx = \frac{h\mu_0}{d^2}J^2 \int_0^\delta \int_0^\delta \frac{1}{\delta^2} dxdx \Rightarrow m\ddot{x} = \frac{\mu_0 h}{2d}J^2 = 1/2 L_1 J^2 \tag{12}$$

where m=total mass acclerated

δ=current zone thickness

L_1=channel inductance per unit length

Also, circuit equation (1) can be written with the capacitor voltage in the form

$$\frac{d}{dt}\left[J\left(L_0+L_1x\right)\right]+JR+\frac{Q}{C}=\left(L_0+L_1x\right)\dot{J}+JL_1\dot{x}+JR-V_0+\frac{1}{C}\int_0^t Jdt=0 \tag{13}$$

Equations (12) and (13) constitute a set of relations in J(t) and x(t) in terms of the parameters m, L_0, L_1, V_0, C and R, assuming R to be constant through the pulse. To simplify the calculations the following nondimensionalization is applied

$$x^*=\frac{L_1}{L_0}x$$

$$t^*=\frac{1}{\sqrt{L_0C}}t \tag{14}$$

$$J^*=\frac{1}{V_0}\sqrt{\frac{L_0}{C}}J$$

to reduce former relations (12) and (13) into

$$\left(x^*\right)''=\alpha\left(J^*\right)^2 \tag{15}$$

$$\left(1+x^*\right)\left(J^*\right)'+J^*\left(x^*\right)'+\beta J^*=1-\int_0^{t^*}J^*dt^* \tag{16}$$

with dimensionless initial conditions

$$
\begin{aligned}
x^*(0) &= 0 \\
(x^*)'(0) &= 0 \\
J^*(0) &= 0 \\
(J^*)'(0) &= 1
\end{aligned}
\tag{17}
$$

where primes indicate derivatives with respect to t^* and α and β are the crucial parameters

$$\alpha = \frac{C^2 {V_0}^2 {L_1}^2}{2mL_0} \tag{18}$$

$$\beta = R\sqrt{\frac{C}{L_0}} \tag{19}$$

In fact, β turns out to be our earlier factor of the damping characteristic in the RCL circuit. Being $\beta \gg 1$, the tendency is toward an overdamped behavior; meanwhile if $\beta \ll 1$ the circuit exhibit an oscillatory waveform. The importance of the dynamic impedance is reflected in the parameter α, that expressed in the following form

$$\alpha = \frac{1}{2}\frac{\left(1/2C{V_0}^2\right)\left(L_1\dot{x}\right)^2}{\left(1/2m\dot{x}^2\right)\left(L_0/C\right)} = \frac{1}{2}\left(\frac{1/2C{V_0}^2}{1/2m\dot{x}^2}\right)\left(\frac{\dot{L}}{R}\right)\beta^2 = \frac{1}{8\pi^2}\left(\frac{1/2C{V_0}^2}{1/2m\dot{x}^2}\right)\left(\frac{2\pi\sqrt{L_0C}}{L_0/\dot{L}}\right)^2 \tag{20}$$

shows four ratios of interest: the ratio of energy initially stored in the capacitance to the kinetic energy transfered to accelerate the mass, which should be around the unity in an efficient accelerator; the ratio of dynamic impedance to circuit resistance, $\dot{L}/R$; the static circuit damping parameter β; and the ratio of the period of the initial circuit, $2\pi\sqrt{L_0C}$, to the unit of time required for the inductance to increase an amount equal to its initial value L_0. Therefore, accelerators with large α are expected to present current waveforms severely damped and protracted in wavelength as time gets consumed.

Numerical resolution of the differential set of equations stated before, eqs.(15-17), confirm the former interpretation of both parameters.

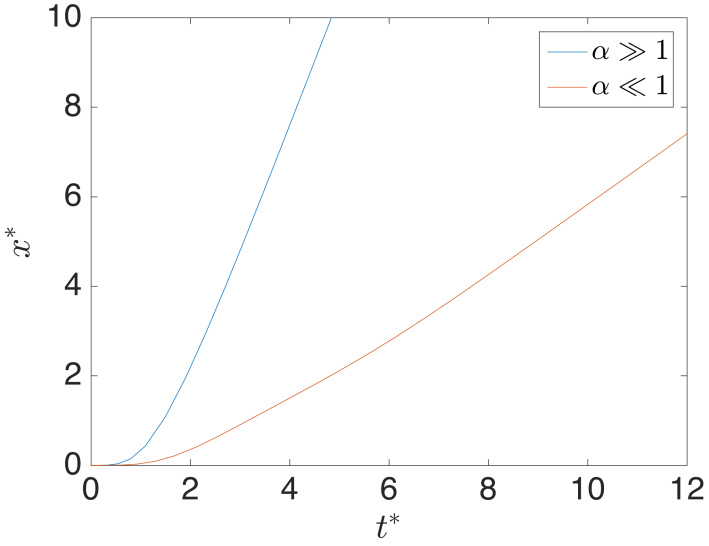

(a) Current sheet trajectory.

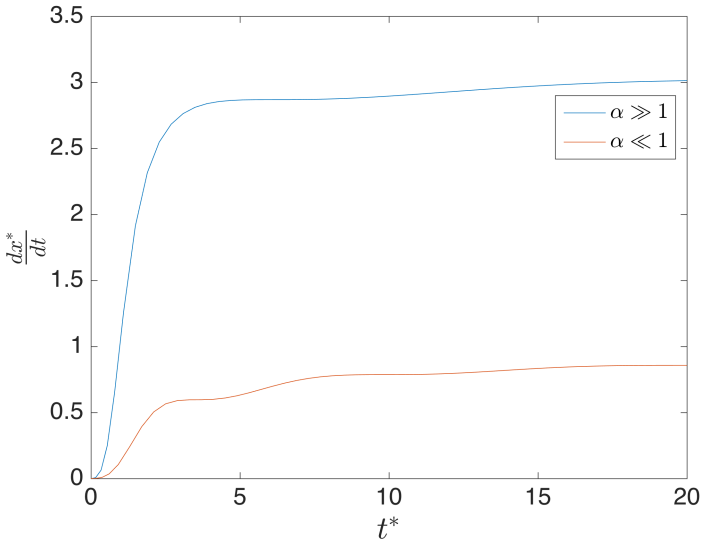

(b) Current sheet velocity.

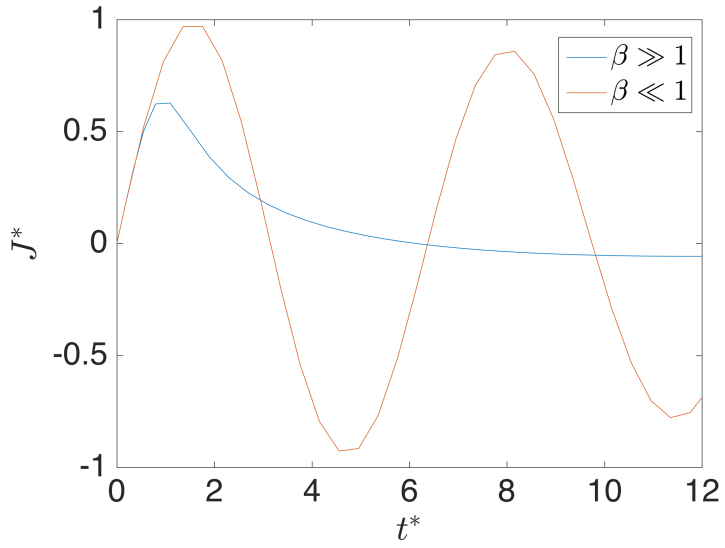

(c) Current waveform.

Figure 18: Dimensionless current waveforms and current sheet trajectories from slug model.

For $\alpha \gg 1$ and $\beta \gg 1$, it can be observed the overdamped behavior in the current waveform $J^*(t^*)$, fig.18(c), and its associated monotonically accelerating slug trajectories $x^*(t^*)$. With this parameters configuration the achieved force is expected to be higher since it is proportional to the acceleration, and this can be estimated as the slope of the velocity, fig.18(c), greater in this situation.

For $\alpha \ll 1$ and $\beta \ll 1$, this time the current exhibits an oscillatory behavior which gets translated in minor fluctuations in the sheet velocity. Nevertheless, these fluctuations are not a main concern since the trajectory keeps augmenting with time.

Applying this analysis it is presumed that the plasma sheet remains coupled to the circuit even after current reversal, so this layer is the one and only element capable of closing the external circuit. But, as mentioned earlier, many experimental investigations shows an important tendency in this PPTs to initiate a new plasma sheet discharge, this will deviate a major part of the circuit current from the primary layer, invalidating the analysis. To take this into account it is needed a more elaborate external circuit.

2.4 Snowplow model

It is obvious that the Slug model, even if simple and helpful, has an important deficiency, it neglects the entrainment of ambient mass as the current sheet propagates through the channel. To reproduce in an effective manner the sweeping process, another analytical model regards the current zone as an impermeable and completely absorbing surface. Therefore, all the mass soaked in the advancing surface is assumed to be fully accumulated within it and travel with it; hence the name "snowplow".

There is no changes in the circuit equation eq.(13), but Newton's law now contains another inertial term for the rate of change of mass:

$$m\ddot{x} + \dot{m}\dot{x} = 1/2L_1J^2 \tag{21}$$

To represent the evolution of mass, the current sheet initially embodies a certain small mass m_0. The existence of this m_0 is experimentally proven and terminate a troublesome singularity when having initially zero mass. After breakdown, and as the current sheet accelerates, it starts to accumulate mass at a rate determined precisely by the velocity, the channel dimensions, and the ambient gas density $\rho(x)$ assumed to be uniform:

$$m(x) = m_0 + hd\int_0^t \rho(x)\dot{x}dt = m_0 + hd\rho x \tag{22}$$

Taking this in consideration, the dynamical equation may be written

$$(m_0 + hd\rho x)\ddot{x} + hd\rho\dot{x}^2 = 1/2L_1J^2 \tag{23}$$

Same nondimensionalization than in the slug model is applied

$$x^* = \frac{L_1}{L_0}x$$

$$t^* = \frac{1}{\sqrt{L_0C}}t \tag{24}$$

$$J^* = \frac{1}{V_0}\sqrt{\frac{L_0}{C}}J$$

Yielding the following dynamical and circuit equations:

$$(m^* + x^*)\,(x^*)'' + \left[(x^*)'\right]^2 = \alpha\,(J^*)^2 \tag{25}$$

$$(1 + x^*)\,(J^*)' + J^*\,(x^*)' + \beta J^* = 1 - \int_0^{t^*} J^* dt^* \tag{26}$$

with dimensionless initial conditions

$$\begin{gathered} x^*(0) = 0 \\ (x^*)'\,(0) = 0 \\ J^*\,(0) = 0 \\ (J^*)'\,(0) = 1 \end{gathered} \tag{27}$$

where

$$\alpha = \frac{C^2 {V_0}^2 {L_1}^2}{2\mu L_0}$$

$$\mu = hd\rho\frac{L_0}{L_1} \tag{28}$$

$$\beta = R\sqrt{\frac{C}{L_0}}$$

$$m^* = \frac{m_0}{\mu} = \frac{L_1 m_0}{hd\rho L_0}$$

As before, numerical computations performed on this model reveals two main differences with respect to the slug model. At a first glance, the current sheet does not present a monotone acceleration across the channel, it absorbs mass more rapidly than the layer's inertia can sustain, and therefore, suffering a deceleration. Secondly, and following this same reasoning, acceleration is notably higher at initial times where the mass accumulated is yet small, and keeps lowering as more mass entrains the sheet. Of course the damping parameters play here the same role as in the slug model.

Comparing with the slug model (dashed line), one can observe the lower value of the velocity reached, considering now increasing mass in the model. Also, the current distribution revealed is slightly lower in their peaks in the snowplow model, another impact of the changing mass.

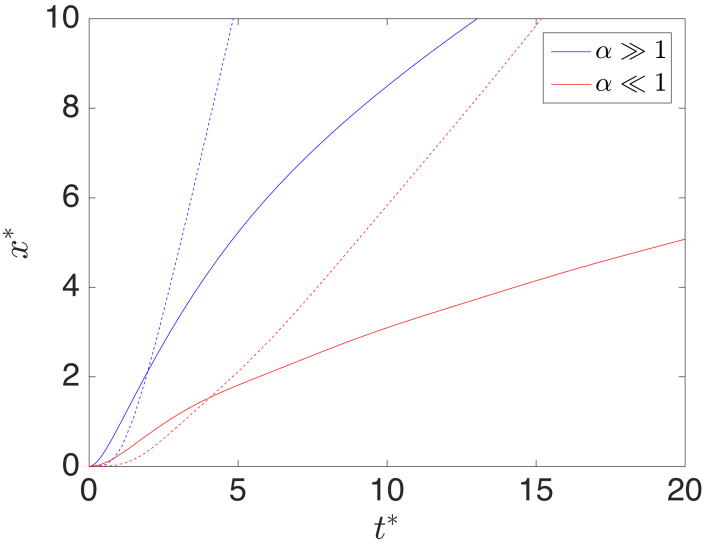

(a) Current sheet trajectory.

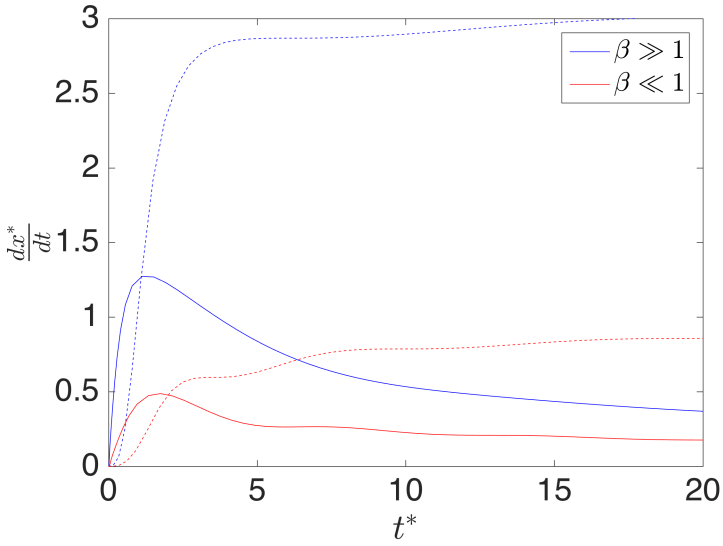

(b) Current sheet velocity.

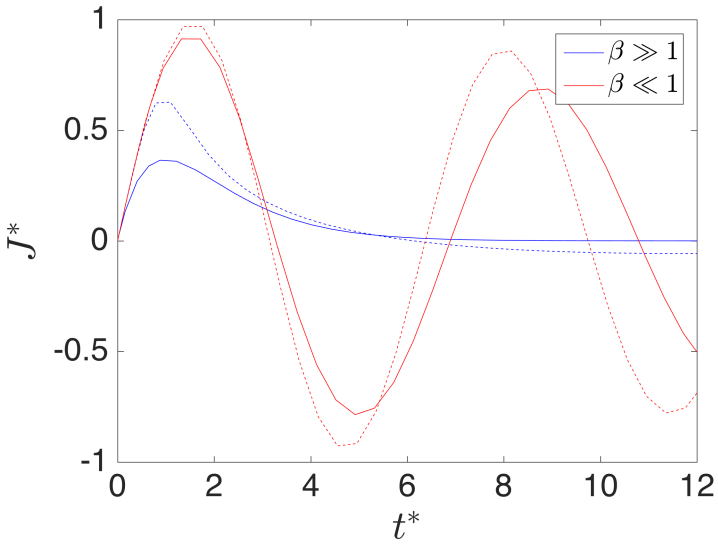

(c) Current waveform.

Figure 19: Dimensionless current waveforms and current sheet trajectories from snowplow model (solid line) and slug model (dashed line).

Snowplow model turns out to be, leaving its assumptions apart, a more than realistic tool to predict current sheet trajectories for PPTs. Same as commented before, many devices of this type present secondary breakdowns with current reversal, and this model does not provide the necessary implementations to take these short-circuiting effects into consideration. But, with the use of a more sophisticated circuit modeling, more accurate results can be obtained. Another typical approach mainly followed in laboratories is to specify the current waveform in advance,

leaving only the dynamical equation eq.(25) to be solved. This can be useful since energy transfer from source to plasma is not the main concern. However, from a propulsion point of view, a precise coupling between the dynamical impedance of the discharge and the output impedance of the source is critical to achieve proper performance results.

3 Performance

3.1 Model performance comparison

Until now, the nondimensional analysis has served perfectly to understand the behavior of PPTs through the comprehension of layer movement and current waveform variations under the influence of the variables α and β.

Now, to analyze the performance of the PPT four critical variables are considered: pulse period (T), impulse bit (I_{bit}), specific impulse (I_s) and efficiency (μ).

The impulse period (T) is the time lapsed by the current sheet to go through the entire channel. To extract precisely this value the simulation of the model has to be stopped once the value of the layer position reaches the end of the channel.

The impulse bit (I_{bit}) is the momentum generated, the mass times the velocity (eq. 29) at the end of the channel, which is, actually, the thrust integrated in a single pulse.

$$I_{bit} = m_f \dot{x}_f = \int_{t_0}^{t_f} F dt \tag{29}$$

The specific impulse is, in fact, the velocity at the exit. Notice that conventionally this impulse is presented in seconds dividing the velocity by the standard gravity ($g = 9.8\, m/s^2$).

$$I_s = \frac{\dot{x}_f}{g} \tag{30}$$

Finally, the efficiency is, of course, nondimensional and measures the ratio between the efficient energy extracted from the PPT and the initial energy discharged by the capacitor. The former is splitted into two main parts: the first one is the energy of the capacitor actually transfered to the electric circuit in form of current

$$E_C = \frac{1}{2}\frac{{Q_f}^2}{C} \tag{31}$$

where $J = -\dfrac{dQ}{dt}$, and the second part is the energy of the capacitor wasted due to resistive losses

$$E_R = \int_0^t J^2 R dt \tag{32}$$

Obviously the sum of the two energies equals the initial energy discharged by the capacitor, the lower term in the definition of the efficiency.

$$E_0 = \frac{1}{2}\frac{{Q_0}^2}{C} \tag{33}$$

The upper term turns out to be simply the kinetic energy transported by the current layer at the end of the pulse, leaving an expression for the efficiency, eq. (34), which can also be expressed in terms of the impulse bit and specific impulse (in m/s).

$$\mu = \frac{1/2 m_f \dot{x}_f^2}{E_0} = \frac{m_f \dot{x}_f^2 C}{{Q_0}^2} = \frac{I_b I_s C}{{Q_0}^2} \tag{34}$$

To implement this performance analysis and to give a sense of scale of all the variables involved, an ablative PPT developed at the university of Tokyo [23] would serve as reference of the approximate values of the different parameters that conform the snowplow model, presented in the following table:

APPT parameters	**Value**
Channel height (h)	20 mm
Channel width (d)	10 mm
Channel length (l)	25 mm
Capacitor (C)	3 µF
Discharge voltage (V_0)	2200 V
Initial mass (m_0)	3.5 µg

Table 2: APPT parameters from university at Tokyo [23]

Nevertheless, there are still some variables to model or estimate, that would be the inductance, the resistance and the density conditions inside the channel.

The inductance per unit length was previously defined in eq.(6).

$$L_1 = \frac{\mu_0 h}{d} \tag{35}$$

However, a more accurate empirically deduced formula is proposed at [10] trying to separate from the quasi-infinite electrode geometry assumption and obtain more realistic results.

$$L_1 = \frac{\mu_0}{\pi}\left[1.5 + \ln\left(\frac{h}{d}\right)\right] \tag{36}$$

Having modeled the inductance per unit length and estimating an initial inductance $L_0 = 2\,\mathrm{p}F$ this parameter gets shaped.

It is important to remind that in this model the plasma resistance is assumed constant, as it is hard to be predicted numerically, many studies analyze the behavior of the resistance throught the pulse. Thanks to his empirical observations, a value of $R = 0.5\,\Omega$ is assessed by P.J.Turchi [40] to be a reasonable value for the resistance.

Lastly, since a snowplow model has been assumed, a density is needed to model the amount of mass swallowed by the current layer on its way through the channel, $\rho = 10^{-5}\,\mu g/mm^3$, which leads to a total increase in mass of 0.05 μg.

Having all critical parameters properly defined, and making use of the relations imposed in eqs. (29-34) the performance results for both slug and snowplow model are presented in table (3):

	$T\,(\mu s)$	$m_0\,(\mu g)$	$m_f\,(\mu g)$	$I_{bit}\,(\mu N - s)$	$\dot{x}_f\,(m/s)$	$I_s\,(s)$	$\mu\,(\%)$
Slug	2.26	3.5	3.5	54.46	15560	1586.7	10.64
Snowplow	2.28	3.5	3.55	54.54	15364	1566.7	10.32

Table 3: Slug-snow performance.

It is important to understand that the reference data of the APPT has been taken to assess the variation in the performance results between both models and not to evaluate its absolute magnitude. Having this in mind, the only difference, as explained previously in the definition of the models, is the implementation in the snowplow of a density that estimates the increase in mass of the current sheet passing through the channel.

As more mass is swallowed by the sheet, more time is needed to transport all this mass to the end of the channel. Of course, the mass variation in the slug equals zero as it is not taken into account

in this model, meanwhile in the snowplow around 1.5 % increase of mass is considered.

The final velocity achieved in the snowplow is slightly lower since a greater amount of mass is needed to be accelerated. Nevertheless, the mass increase weights more than the velocity decrease leading to a momentum increase, eq.(29), getting therefore more impulse bit in the snowplow.

In terms of efficiency, considering the second term of eq.(34), the final velocity is squared in the expression gaining more importance in comparison with the mass. Therefore, the efficiency in the snowplow gets reduced, this has logical sense since considering an amount of mass that is entering in the current sheet makes the model less ideal or more realistic, less efficient.

Needless to say that increasing the density ρ make these differences between models greater.

3.2 Key parameters

In this section, now that the main performance variables have been defined and the differences between models have been perfectly understood, it is time to analyze the response of the performance when varying certain key parameters, to be chosen when designing a proper PPT.

The parameters considered are: initial mass (m_0), initial voltage (V_0), capacitor (C) and channel length (l). Again, eqs.(29-34) are applied to obtain results of the pulse period (T), impulse bit (I_{bit}), specific impulse (I_s) and efficiency (μ).

It is important to clarify that, when varying a certain parameter, all the rest of variables in the model remain unchanged to assess, in this way, the performance response with respect to the variation of each key parameter.

3.2.1 Initial mass

The initial mass extracted from the propellant (Teflon) is a matter of extreme complexity left out of the scope of this paper, several experimental based ablated models have been studied trying to replicate as similar as possible this intricate process.

The importance of this parameter is huge, varying the value for the initial mass, the whole performance of the PPT gets dramatically changed.

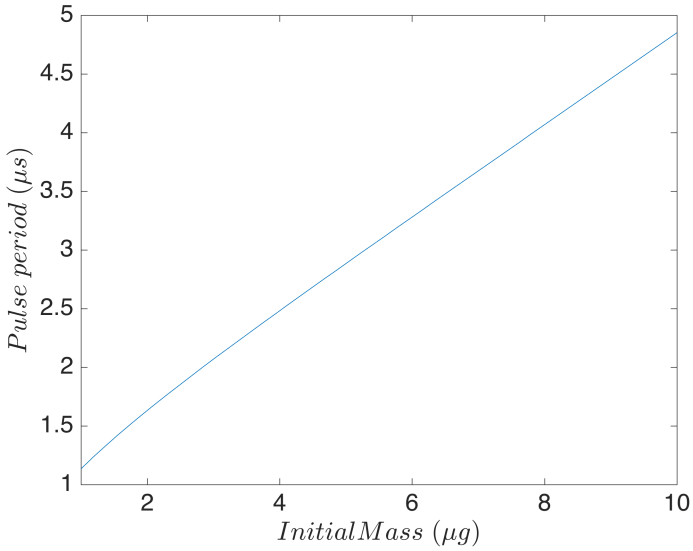

(a) Pulse period.

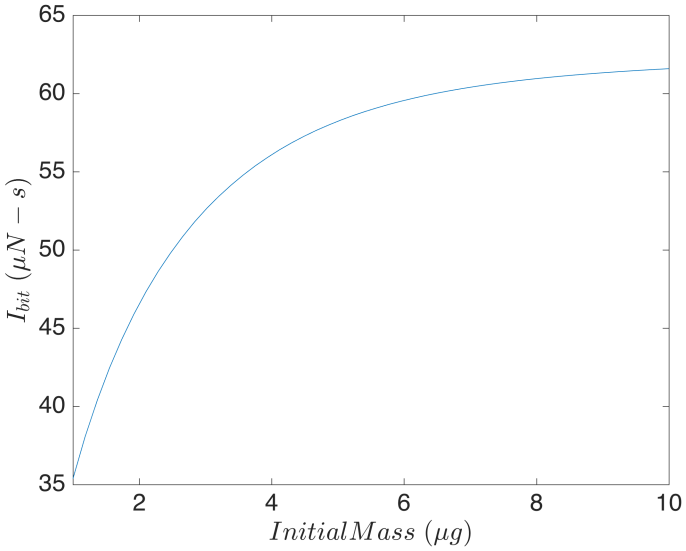

(b) Impulse bit.

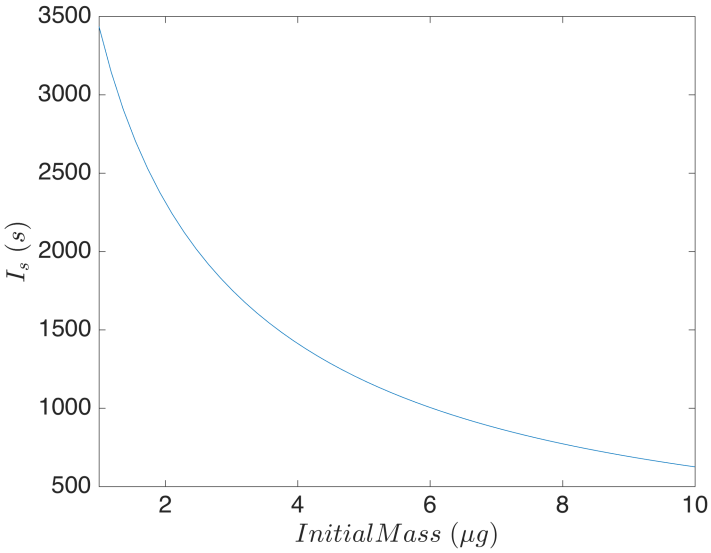

(c) Specific impulse.

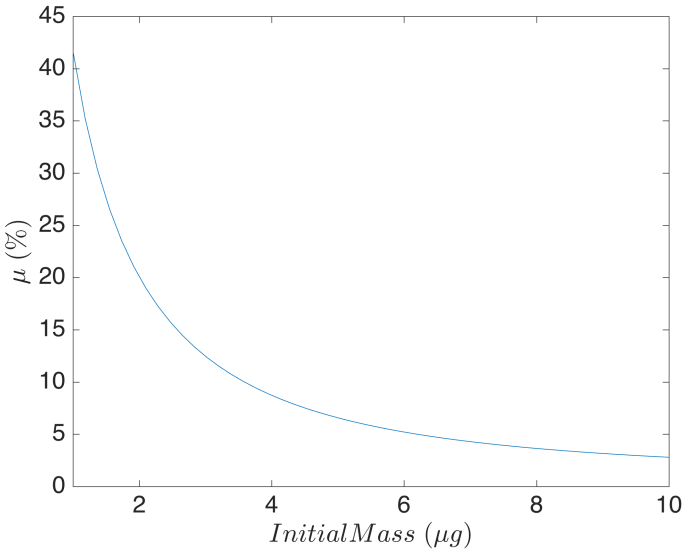

(d) Efficiency.

Figure 20: Performance analysis varying initial mass.

In fig. (20) it is observed that, augmenting the mass, the time needed for the current sheet to reach the end of the channel increases linearly. Meanwhile, the impulse bit has more an increased curve tendency that almost gets established around certain value when increasing the mass. This same behavior is observed in the specific impulse and efficiency, but in opposite sign, decreasing both parameters.

The key here lies in the $I_{bit} - \mu$ or $I_{bit} - I_s$ straighten. Moving a greater amount of mass, more

thrust is obtained but with a penalizing reduction in efficiency and exit velocity. In the other way around, only a great efficiency can be achieved with low values for the impulse bit and exit velocity. The point is all have a tendency response, so impulse bit, efficiency and specific impulse change rapidly at the beginning and then gets almost steady, having no need to increase the initial mass to more than 5 μg in this particular situation.

3.2.2 Initial voltage

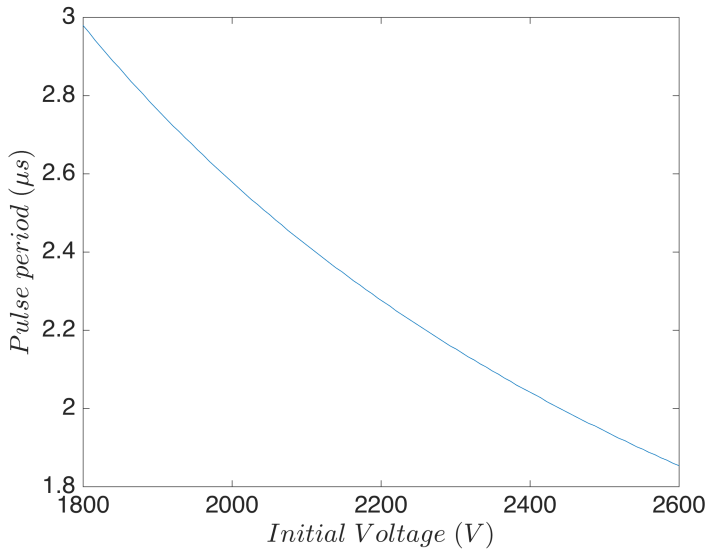

(a) Pulse period.

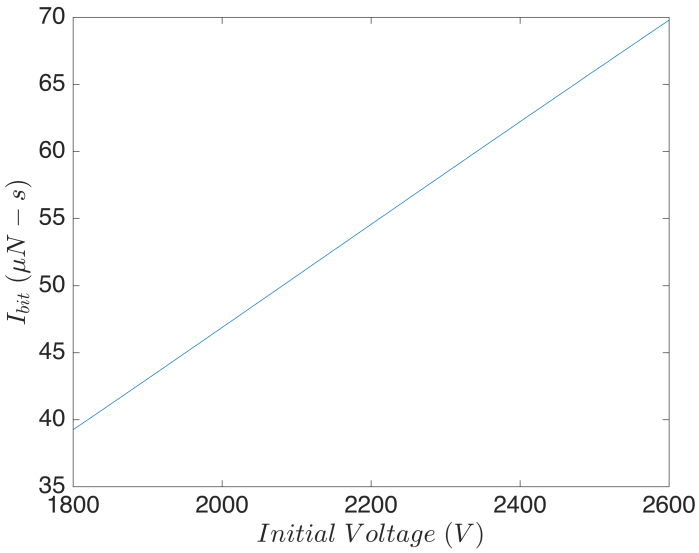

(b) Impulse bit.

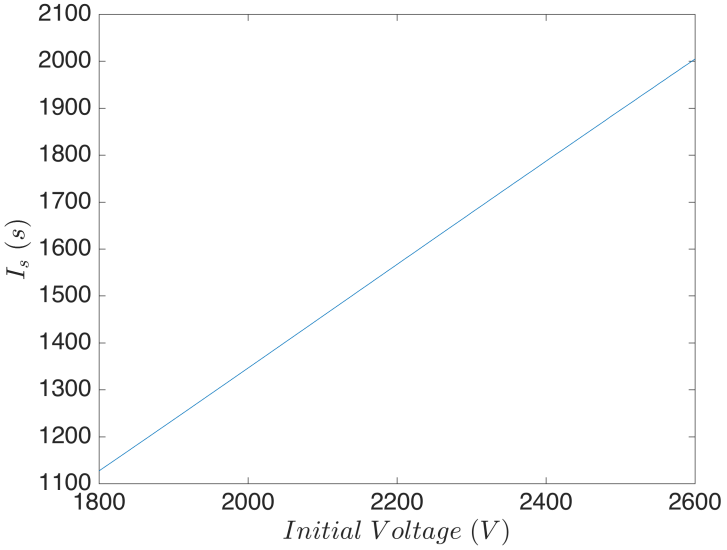

(c) Specific impulse.

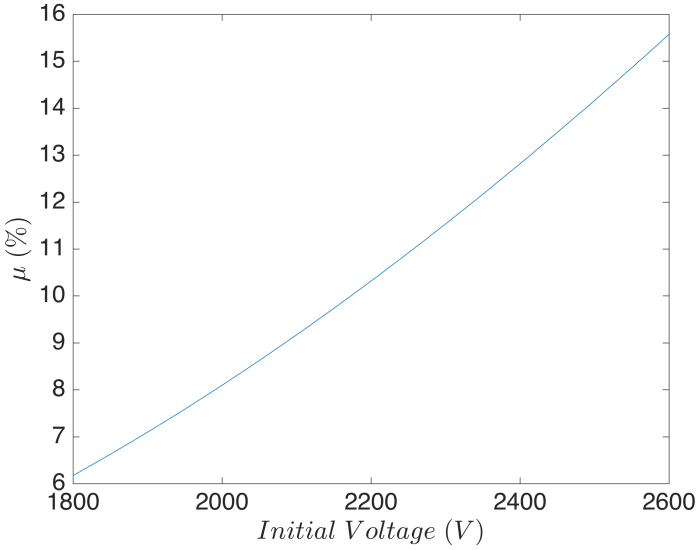

(d) Efficiency.

Figure 21: Performance analysis varying initial voltage.

The importance of this parameter gets clearly shown taking a look at figure (21) where it is observed that increasing the initial voltage favors almost linearly every performance parameter. The pulse period gets decreased with a more curvilinear behavior, the impulse bit and the specific impulse increases linearly and the efficiency increases with a flat curve tendency.

This behavior gets perfectly understood in eq.(13) where an increase in the initial voltage affects directly and in a positive way both the current sheet velocity and current variation.

Nevertheless, it has to be noticed that this initial voltage is limited to a certain maximum allowed depending on the capacitor allocated, surpassing this maximum allowed voltage would usually result in the destruction of the capacitor.

3.2.3 Capacitor

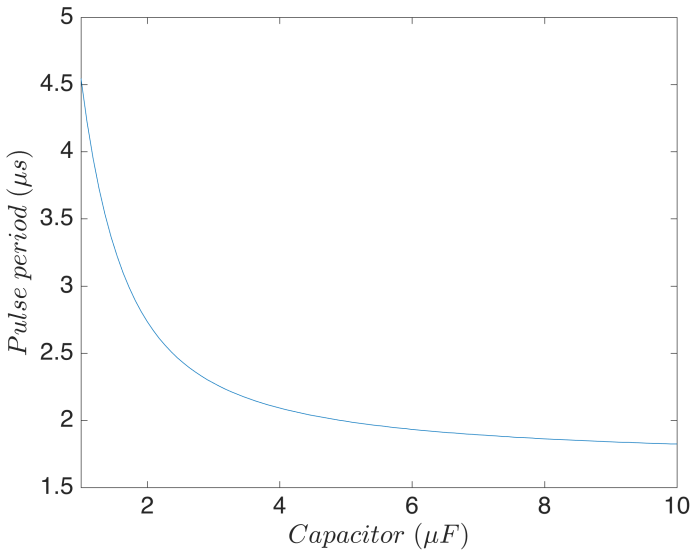

(a) Pulse period.

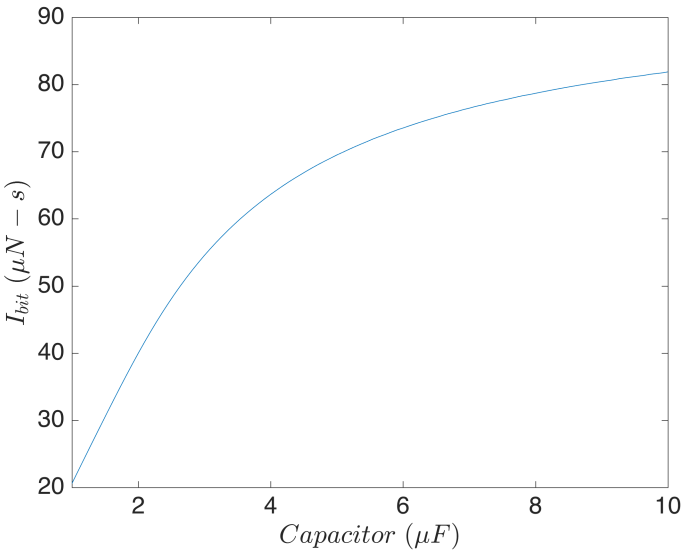

(b) Impulse bit.

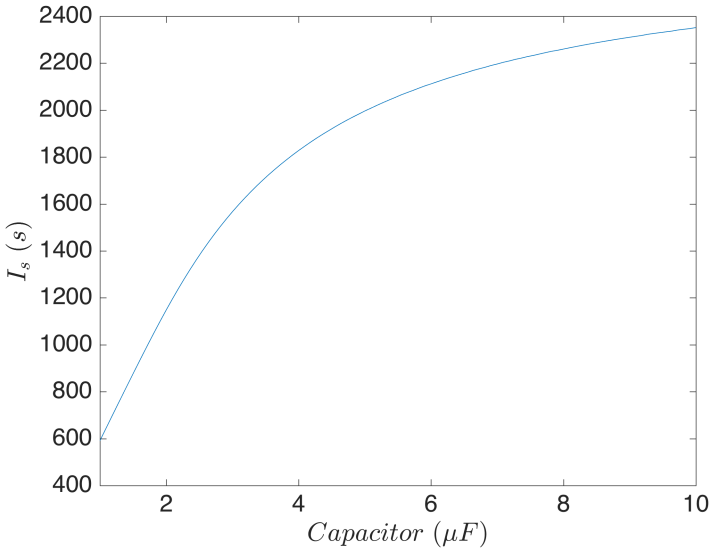

(c) Specific impulse.

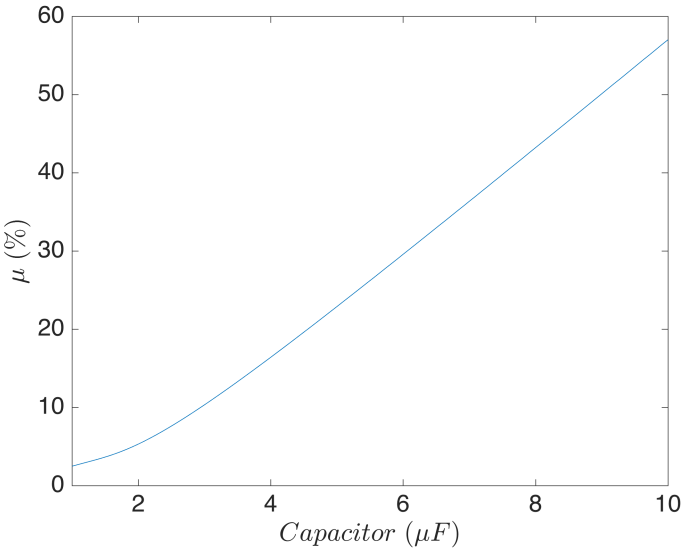

(d) Efficiency.

Figure 22: Performance analysis varying capacitor.

The capacitor ability is critical, it enables, when increased, great impovements in performance. Coming back again to eq.(13), C is located at the denominator giving us expectations of what is captured in fig. (22). The I_{bit} and I_s increases in a curvilinear behavior, the efficiency does as well but with a less curved tendency, and since the velocity at the exit is increased, the time needed for the layer to go through the channel gets lowered substantially.

Notice that the curves, excluding the efficiency one, have a tendency to a certain value. For this reason it is not a good decision to keep augmenting the capacitor more than 5 µF.

However, the capacitor ability is obviously positively related with its mass and volume. Therefore, capacitors with more than 4 µF are not common in this type of thrusters. The presence of a bank of capacitors is usually adopted to try to optimize the volume available and to give some reliability in case of failure of one capacitor.

3.2.4 Length

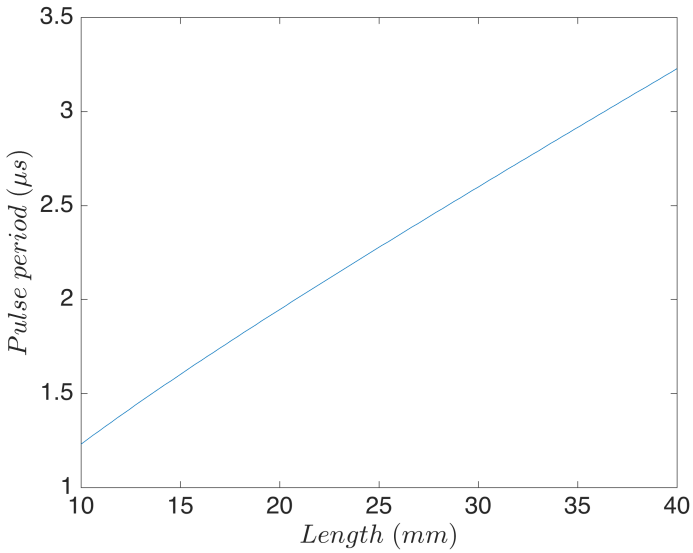

(a) Pulse period.

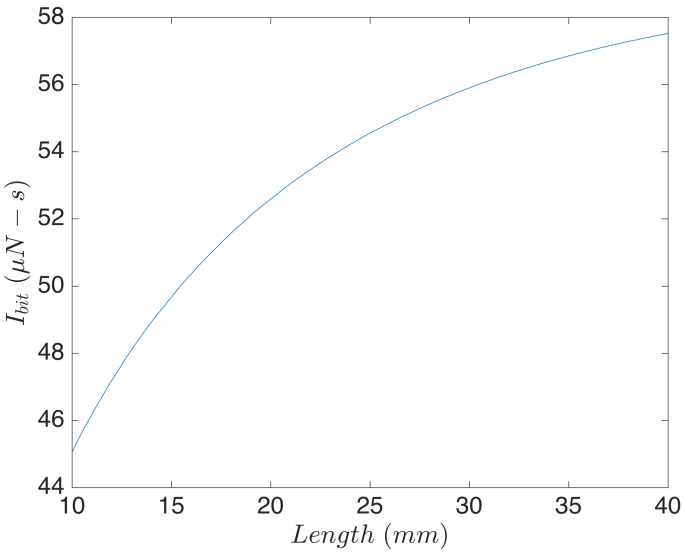

(b) Impulse bit.

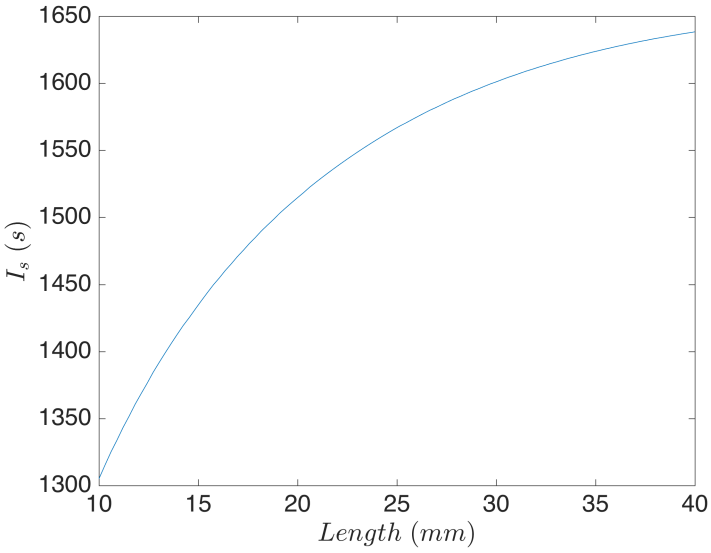

(c) Specific impulse.

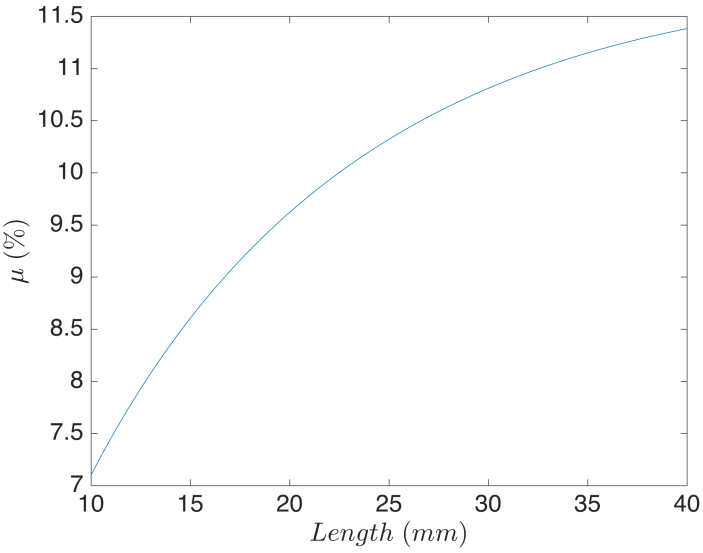

(d) Efficiency.

Figure 23: Performance analysis varying channel length.

Channel length turns out to play a key role in here as well. It is obvious that as more distance is needed to cover more time is needed too. Since there is more time to accelerate the current sheet, the final velocity or specific impulse achieved is higher following a curvilinear behavior with some tendency, it grows rapidly at the beginning but gets stabilized, so there is no point on designing a too long PPT. The impulse bit, since the final velocity gets increased plus the mass swallowed is

greater as well, follows a similar behavior. Having a too large channel also increases the efficiency as it is linearly dependent to the kinetic energy at the exit, eq.(34).

Ideally, a PPT as long as possible would imply a greater PPT performance in a lower response (greater T). But, to be used in nanosats, demanding constraints of mass and volume have to be fulfilled so this constitute the main limitation of the total length of the channel.

3.3 Flared improvement

Flared PPTs are, in fact, an improvement already implemented in actual designs, as observed in figure (7) previously included when introducing PPTs. To model this, an angle ϵ is defined as the angle that forms the plate direction with the horizontal, being:

$$\tan\epsilon = \frac{h_f/2 - h_0/2}{l} = \frac{h_f - h_0}{2l} \tag{37}$$

With this simple relation an expression of the height as a function of the current sheet position is obtained.

$$h(x) = h_0 + 2x\tan\epsilon \tag{38}$$

To have a flared ratio h_f/h_0 of around 1/2 the angle ϵ would be approximately 12° following our reference geometrical parameters, table 2.

Actually, introducing a variable height across the channel makes inductance per unit length no longer a constant value, eq.(36). Introducing this aspect in the model, the obtained results are reflected in fig.(24).

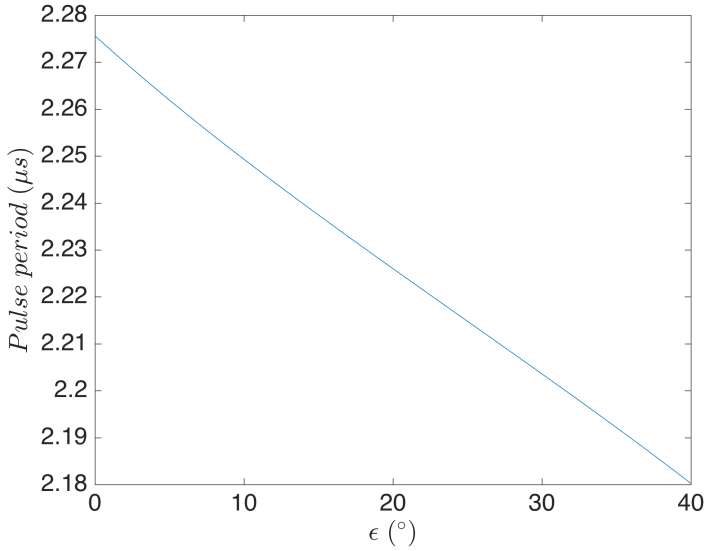

(a) Pulse period.

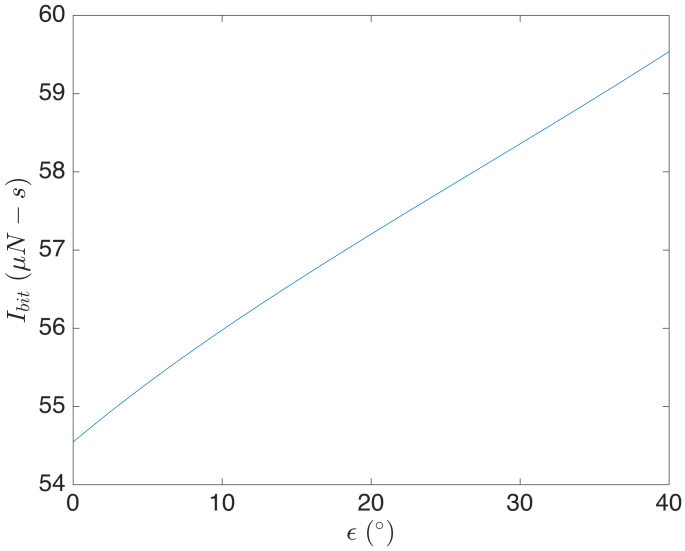

(b) Impulse bit.

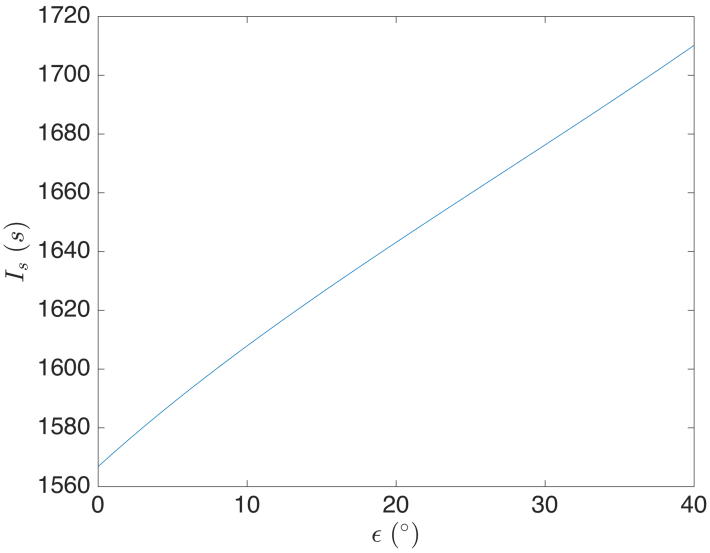

(c) Specific impulse.

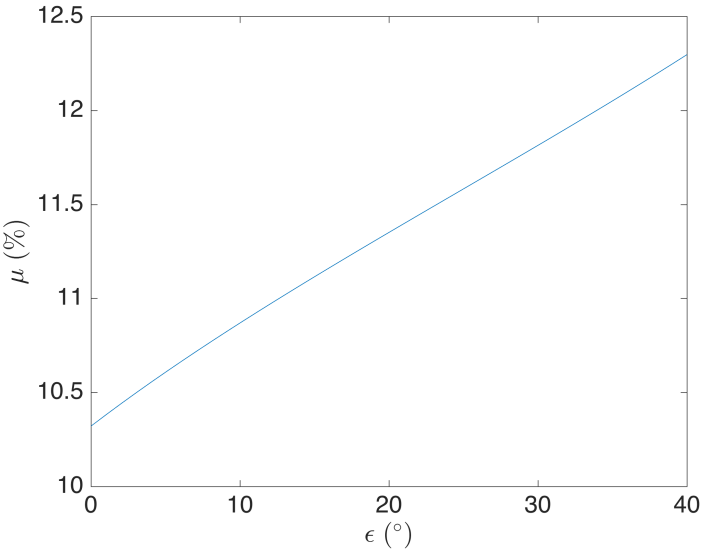

(d) Efficiency.

Figure 24: Performance analysis varying taper angle.

The results turn out to be excellent. When having the reference design commented previously, and introducing a flare angle up to 40° the pulse period suffers a reduction of a 4%, the impulse bit grows about an 8% and the specific impulse increases around 150 s. Additionally, the efficiency increases about 1.8%.

The only drawback of this implementation is a slight increase in mass since the actual plates are longer.

Empirically, presented in [1], the flared design implies an inductance increase, as taken into account in here, but also an increase in the resistance, in the mass ablated and a poor propellant utilization. Therefore, through experimental testings performed in the National University of Defense Technology, the overall performance gets improved for increasing flare angles until reaching a maximum that is around 27°.

This last peak in the flare angle is not revealed with our model since the resistance is assumed to be constant and the mass ablated is left constant too, leaving behind two important aspects empirically proven but not considered in here.

Nevertheless, for flare angles up to 27° the model still provides a good approximation of the performance improvement when including this configuration.

4 Final design

In this section, all the knowledge acquired is going to be put together to design an actual µPPT that accomplish some particular specifications.

4.1 Mission requirements

The µPPT will be used in a 3U cubesat. Typically, both the thruster and its electronics are mounted on a PCB card with standard dimensions, a PC104 [13] card provides for the propulsive system of the cubesat a 90 x 90 x 90 mm volume. The thrust direction is chosen to be along the 27 mm direction to optimize this distance and leave the other two to fit all the electronics. Given a thickness for the PC104 card of 1.6 mm, the channel length would be equal to 25 mm.

Taking into account the limitations in weight when dealing with cubesats, for this 3U cubesat ($\approx 3\,\text{kg}$) only 150 g are assigned for the propulsion system, out of which around 5 g of propellant can be allocated.

The thruster will have the crucial task of compensating the induced drag maintaining the cubesat in orbit. The satellite has to be able to perform its orbital trajectory at a nominal altitude of 600 km during, at least, 3 years.

Considering the equality that takes place in satellite orbits between its weight and the centripetal force suffered, an expression for its velocity is easily derived.

$$Mg = M\frac{v^2}{R} \Rightarrow v = \sqrt{gR} = 8265\,m/s \tag{39}$$

Notice that in expression (39) the term R gets defined by the addition to the 600 km altitude of the earth's radius (6371 km).

To calculate the drag force induced the area of contact is set to be the wider face of the cubesat (10 x 30 mm), the drag coefficient is assumed to be equal to 2.2 and the density is estimated as $\rho = 5 \cdot 10^{-13}\,kg/m^3$. The density is, in fact, an average density at this height since the radiation from the sun expands the earth's outer atmosphere increasing the drag induced in satellites, a phenomena object of many studies and left behind the scope of this paper.

$$F_d = 1/2\rho A C_D v^2 = 0.51\ \mu N \tag{40}$$

Multiplying this drag force by the total life time of the satellite (3 years) an overall total impulse of 48.52 µN-s must be delivered. For an amount of mass of propellant to be loaded in the thruster equal to 5 g, the average specific impulse to target for the µPPT is equal to $I_s = 990s$.

All the mission requirements get summarized in table 4.

Requirement	**Value**
Volume	90 x 90 x 27 mm
Channel length	25 mm
Propellant mass	5 g
Life time	3 years
Total impulse	48.52 µN-s
Specific impulse	990 s

Table 4: Mission requirements.

4.2 Model optimization

To try to find an optimum design the snowplow model presented previously is going to be taken back in here with its non dimensional variables α and β. It is important to have in mind their definitions during this section, eq.(28).

The performance parameters studied before: pulse period (T), impulse bit (I_{bit}), specific impulse (I_s) and efficiency (μ), are going to be plotted as contour lines in a $\alpha - \beta$ mesh to study the existence of an optimum ideal design point.

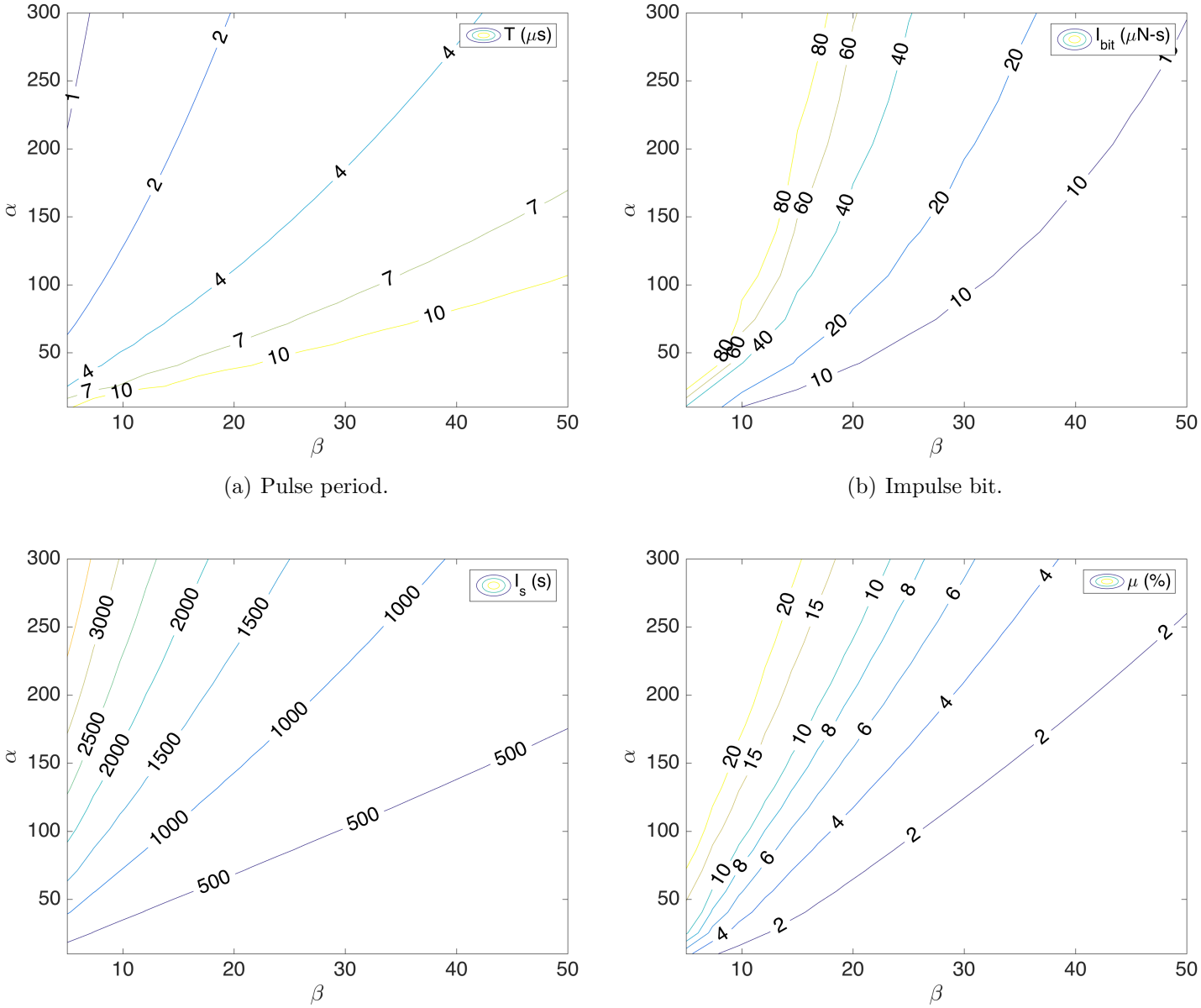

(a) Pulse period.

(b) Impulse bit.

(c) Specific impulse.

(d) Efficiency.

Figure 25: Performance contours in $\alpha - \beta$ mesh.

As could have been expected, fig. (25) shows no enclosed area in which the performance reaches its maximum. Instead of that, it seems that having a value for α as high as possible and for β as low as possible enhances the overall performance by reaching the highest values of impulse bit, specific impulse and efficiency in the shortest period times of execution.

But, there exist an important limitation already explained in this paper when defining the circuit model. For values of $\beta \ll 1$ the current gets an underdamped behavior capable, for low enough

values, to cause large oscillations and an induced current sheet reversal entering in a not well-known domain uncovered by this model.

On the other hand, the value of α cannot reach too high values since it is quadratically defined by the capacitor (C) and the initial voltage (V_0), both constrained by the mass limitations and further capacitor technology advances.

4.3 Design performance

Checking fig. (25), values of $\beta = 20$ and $\alpha = 165$ seem reasonable to aim the mission requirements with some safety margin.

For this β, and assuming as in previous chapters a resistance of 0.5 Ω and an initial inductance equal to 2 pH, the capacitor needs to provide 3.2 µF. This can be easily achieved with a capacitor bank using four 0.8 µF capacitors able to withstand up to 2000 V.

For this value of α, keeping a height of 20 mm and a width of 10 mm, reasonable geometrical values given the limited volume for the propulsive system, and assuming a mass bit in every pulse equal to 3.5 µg; an initial voltage of 1730 V, inside limitations, would be required to be accurately positioned in the design point chosen.

Having defined all the parameters that drives the thruster, the performance at its design point is reflected in table (5). When introducing the flared improvement the final design gets completed.

	$T\ (\mu s)$	$I_{bit}\ (\mu N - s)$	$I_s\ (s)$	$\mu\ (\%)$
Parallel	3.06	38.5	1106	6.11
Flared (25°)	2.97	40.8	1172	7.01

Table 5: Parallel-tapered design point performance.

As observed in the table, flared geometry shows again clear improvements in the performance parameters, leaving no option but to choose flared design as the final one.

At its design point the µPPT thruster is going to deliver an impulse bit of 40 µN-s and an specific impulse of 1172 s, all in a period pulse equal to just 3 µs and with a modest efficiency of 7%. This performance satisfies the specific impulse requirement with a safety margin of 11% taking

into account 5 g of propellant mass and an operation during 3 years as stated in the mission requirements.

This design also accomplish the need of a large enough value of β to avoid current reversal and also considers a cautious value for α so the capacitor bank does not add too much weight to the propulsion device.

4.4 Electronic design

The µPPT electronics are key to charge the capacitors and spark plug and coordinate both circuits. New innovative enterprises such as Clyde Space Ltd [2] provide a clever and refined solution offering the actual entire platform of a cubesat, with all the electronics in board.

Usually, what is called a flyback converter is used to charge the bank of capacitors. To control its voltage (≈1000-2500 V) a simple rheostat can be placed, a rheostat is a typical variable resistor used to control current and, therefore, voltage. It is widely used as power control devices, for example to control light intensity, speed of motors, ovens, etc.

The spark plug needs a larger amount of voltage, up to 15 kV. For this same reason a Cockroft-Walton voltage multiplier is commonly used, it consists, basically, in a network of capacitors and diodes that convert an input low-voltage signal into a high-voltage one.

As mentioned, for a correctly functioning of the firing process, an exact synchronization is demanded. To assure the coordination between both electrical circuits, a µ-controller is used, a small computer in a single integrated circuit.

5 Conclusions and future work

PPTs have been proven as a smart choice of propulsion device to be installed on cubesats. Among its competitors, they stand out because of the simplicity of its design, the very precise control in thrust through the pulsed frequency and its well-known heritage in space flights, due to these reasons µPPTs constitute an economic, reliable and effective solution to the orbit and attitude correction problem.

Defining an inductance-capacitance-resistance (LCR) series circuit a first glance of the functioning of PPTs have been understood, estimating a simple but useful expression for the electrical efficiency that shows us the need to obtain great inductance change rates. Through this analysis two main domains of current have been clarified: an underdamped and an overdamped behavior, separated by the critical case. The non-oscillatory overdamped response is the one sought for, at least, from a circuit analytical point of view.

The slug model adds to the circuit equation the dynamics of the current sheet and presents the interesting non dimensional parameters α and β that have helped to understand the current and layer movement. A large value for α and an overdamped ($\beta \gg 1$) yield the best results.

The main lack of the slug model, the assumption of no mass entraining in the current sheet, has been erased in the snowplow model with the sweeping process through the definition of a density in terms of volume inside the channel. The results differ slightly, due to the augment in mass through the displacement of the layer, the current sheet acceleration is lower and less velocity magnitude is achieved. Snowplow model has proven to be a more accurate replica of reality.

The main performance parameters (T, I_{bit}, I_s and μ) have been formulated and estimated for both models and taking as reference an actually tested APPT [23] to give a first look into the scale of the main variables driving the functioning of this type of thrusters. Of course, the snowplow has resulted in a lower exit velocity and efficiency, but, due to the mass gain, in a higher impulse bit.

The mass ablated has been found to benefit the impulse bit results, but lowering the exit velocity and efficiency needing the current sheet more time to go through the channel. Therefore, a trade-off between either I_{bit} or I_s and μ has to be decided at a design state. The estimation of the mass ablated depending on the conditions given is left out of the scope of this paper, but with the help of a conscious way of modeling this, introducing it in the snowplow model would be done with

relative ease and would provide an improvement in the accuracy of the results.

The initial voltage and capacitor ability, both, have a great impact on the overall performance when increased. The main difference lies in the more rectilinear behavior observed in V_0 compared with the curved capacitor tendency. The conclusion is that increasing the initial voltage seems to increase the performance, ideally, with no limits, meanwhile the capacitor ability reaches a value at which makes no sense to keep augmenting its value. Anyway, these two variables are restricted due to the mass constraints (C) and also because of the functioning of the capacitors up to a certain voltage.

The channel length, again, benefits the performance of the thruster, with the only drawback of implying an increase in the pulse period. There exists also a certain tendency but, not as marked as it was in the capacitor. And, obviously, this length is constrained by the actual dimensions for the µPPT to fit in.

An improvement in the model has been applied adding a geometrical change: flaring. This configuration is widely used in this type of thrusters and with this simple model has been proven to be an easy way of giving an extra amelioration in the performance parameters. Nevertheless, and due to the inconsistency of the constant resistance and non modeled ablated mass assumptions, the performance increase does not seem to cease with the flare angle while in the literature [1] experimental studies prove that there exist some maximum value for this angle from which the performance gets no longer improved, around 27°.

Having defined all the tools needed to model a µPPT, the mission requirements presented constitute the common requisites for an actual cubesat put into space nowadays. The specific impulse to aim is 990 s. The snowplow model is then optimized through the use of performance contours in a $\alpha - \beta$ mesh discovering that the best performance area takes place when increasing α and decreasing β. The value of β has already proven to be not that low from an electric circuit perspective, an oscillatory behavior would produce current reversal. And, the value of α cannot be increased no strings attached since it would imply too big and heavy capacitors.

The design point is chosen to be $\beta = 20$, $\alpha = 165$, providing enough performance results to accomplish the mission, $I_s = 1172s$ and $I_{bit} = 40\mu N - s$ with modest efficiency, $\mu = 7\%$. The electronics needed to charge the capacitors and spark plug and to synchronize the firing process have also been detailed.

Going through these models has been a relatively easy way of understanding the functioning of µPPT and its configuration for certain applications. Nevertheless, through this process these models have been found not to be perfect. This opens up a wide range of future work.

An implementation of a non constant expression for the resistance and a determination of the ablated mass would constitute a significant improvement of this work. Also, to account for secondary breakdowns, a more sophisticated electric circuit, [10], can be combined with exactly the same dynamics to provide more accurate results.

The next step would be now to, having this work as foundation, construct an actual µPPT and, making use of the vacuum chamber available at the installations of UC3M, test it to verify the conclusions extracted in here. The, already explained, simplicity of this thruster makes its construction and testing relatively plain.

In addition, the economics are favorable. A Teflon bar bigger enough to provide for multiple tests would cost 20€. All the capacitors, batteries, the flyback converter, the spark plug, the voltage multiplier, the rheostat and the µ-controller would cost no more than 200€. This economic aspect makes PPTs really affordable to test.

The basics of the µPPT has been understood, its performance, analyzed, and its effectiveness on mission, proven. But there are still many open paths to go through in the development of this type of thrusters.

References

[1] Zhang, R., Zhang, D. X., He, Z., Zhang, F. and Wu, J. J., *Influence of Electrode Flare Angle on the Performance of Pulsed Plasma Thruster*, in Applied Mechanics and Materials (Vol. 232, pp. 353-358). Trans Tech Publications, 2012.

[2] Guarducci, F., Coletti, M. and Gabriel, S. B., *Design and testing of a micro pulsed plasma thruster for Cubesat application*, in 32nd International Electric Propulsion Conference (pp. 2011-239), 2011.

[3] Guarducci, F., Coletti, M. and Gabriel, S. B., *A micro PPT for Cubesat application: Design and preliminary experimental results*, Acta Astronautica, 69(3-4), 200-208, 2011.

[4] Krejci, D., Seifert, B. and Scharlemann, C., *Endurance testing of a pulsed plasma thruster for nanosatellites*, Acta Astronautica, 91, 187-193, 2013.

[5] Williams, D., *Propulsion solutions for Cubesats and applications*, in CubeSat Developers Workshop, Logan, UT, 2012.

[6] THE SUNGKYUN TIMES, *CubeSat: The Ultra-small but Ultra-efficient Artificial Satellite*, found in: http://m.skt.skku.edu/news/articleView.html?idxno=421, 2018.

[7] S. Barral, J. Kurzyna, A. Szelecka, H. Rachubinski, D. Danilko, R. Martin, E. Remirez, P. Ortiz, J. Alonso, Y. Mabillard, S. Bottinelli, A. Zaldivar, P. Rangsten and C. R. Koppel, *Time-of-Flight Spectrometry and Performance of a Pulsed Plasma Thruster with Non-Volatile Propellant*, in Proceedings of the 34th International Electr. Propuls. Conference, Kobe, Japan, 2015.

[8] Zhang, R., Zhang, D. X., He, Z., Zhang, F. and Wu, J. J., *Influence of Electrode Flare Angle on the Performance of Pulsed Plasma Thruster*, in Applied Mechanics and Materials (Vol. 232, pp. 353-358), 2012.

[9] Scougal, E. A., Marchetto, J. D. and Eslava, S. A., *Design of a micro-Pulsed Plasma Thruster for a 3U Cubesat*, 2014.

[10] Burton, R. L. and Turchi, P. J., *Pulsed plasma thruster*, Journal of Propulsion and Power, 14(5), 716-735, 1998.

[11] Cassady, R. J., Hoskins, W. A., Campbell, M. and Rayburn, C., *A micro pulsed plasma thruster (PPT) for the" Dawgstar" spacecraft*, in Aerospace Conference Proceedings, 2000 IEEE (Vol. 4, pp. 7-14), 2000.

[12] Ciaralli, S., Coletti, M. and Gabriel, S. B., *Results of the qualification test campaign of a Pulsed Plasma Thruster for Cubesat Propulsion (PPTCUP)*, Acta Astronautica, 121, 314-322, 2016.

[13] Guarducci, F., Coletti, M. and Gabriel, S. B., *Design and testing of a micro pulsed plasma thruster for Cubesat application*, in 32nd International Electric Propulsion Conference (pp. 2011-239), 2011.

[14] Krejci, D., Seifert, B. and Scharlemann, C., *Endurance testing of a pulsed plasma thruster for nanosatellites*, Acta Astronautica, 91, 187-193, 2013.

[15] Zachary Riley, *NASA Set To Use RS-25 Engine To Extend Our Reach Into Space*, found in: https://www.valuewalk.com/2018/02/nasa-set-use-rs-25-engine-extend-reach-space/, 2018.

[16] Ou, Y., Wu, J., Zhang, Y., Li, J. and Tan, S., *Theoretical Modeling and Parameter Analysis of Micro-Pulsed Plasma Thruster*, Energies, 11(5), 1146, 2018.

[17] Gatsonis, N. and Yin, X., *Particle/fluid modeling of pulsed plasma thruster plumes*, in 35th Joint Propulsion Conference and Exhibit (p. 2299), 1999.

[18] Haag, T. W., *Thrust stand for pulsed plasma thrusters*, Review of Scientific Instruments, 68(5), 2060-2067, 1997.

[19] Huang, T., Wu, Z., Liu, X., Xie, K., Wang, N. and Cheng, Y., *Modeling of gas ionization and plasma flow in ablative pulsed plasma thrusters*, Acta Astronautica, 129, 309-315, 2016.

[20] Pottinger, S. J. and Scharlemann, C. A., *Micro pulsed plasma thruster development*, in 30th International Electric Propulsion Conference, IEPC-2007-125, 2007.

[21] Gibbon, D., Baker, A., Coxhill, I. and Sweeting, M., *The development of a family of resistojet thruster propulsion systems for small spacecraft*, 2003.

[22] Uluşen, D., Aydin, B. Ç., Gülle, İ. S., Bozkurt, E., Özkaya, H., Ontaç, S. and Türkmenoğlu, M. , *Overview of TUBITAK UZAY's electric propulsion development*

project (HALE), in Recent Advances in Space Technologies (RAST), 2013 6th International Conference on (pp. 643-647). IEEE, 2013.

[23] Koizumi, H., Noji, R., Komurasaki, K. and Arakawa, Y., *Plasma Flow Behaviors and Their Effects on the Performance of Pulsed Plasma Thrusters*, in Proceedings of the 30th International Electric Propulsion Conference, Florence, Italy (pp. 17-20), 2007.

[24] Henrikson, E. M., Mikellides, P. G. and Kamhaw, H., *Experimental and Numerical Characterization of an Ablation-fed Pulsed Plasma Thruster Prototype*, in Proc. of 31st International Electric Propulsion Conference, University of Michigan, Ann Arbor, MI. IEPC-2009-246, 2009.

[25] Kang, B., Low, K. S., Soon, J. J. and Tran, Q. V., *Single-Switch Quasi-Resonant DC–DC Converter for a Pulsed Plasma Thruster of Satellites*, IEEE Transactions on Power Electronics, 32(6), 4503-4513, 2017.

[26] Markusic, T. E., Thio, Y. C. F., Cassibry, J. T. and Rodgers, S. L. , *Design of a high-energy, two-stage pulsed plasma thruster*, 2002.

[27] Misra, K., *Multiple Plasma Stream Electromechanical Model for Pulsed Plasma Thruster*, arXiv preprint arXiv:1804.08568, 2018.

[28] Nawaz, A., Lau, M., Herdrich, G. and Auweter-Kurtz, M., *Investigation of the magnetic field in a pulsed plasma thruster*, AIAA journal, 46(11), 2881-2889, 2008.

[29] Nawaz, A., Albertoni, R. and Auweter-Kurtz, M., *Thrust efficiency optimization of the pulsed plasma thruster SIMP-LEX*, Acta Astronautica, 67(3-4), 440-448, 2010.

[30] Jahn, R. G., *Physics of electric propulsion*, Courier Corporation, 2006.

[31] Lemmer, K., *Propulsion for cubesats*, Acta Astronautica, 134, 231-243, 2017.

[32] William Graham , *Arianespace Vega rocket launches Mohammed VI-A*, found in: https://www.nasaspaceflight.com/2017/11/arianespace-vega-mohammed-vi-a-launch/, 2017.

[33] Scharlemann, C., Tajmar, M., Vasiljevich, I., Buldrini, N., Krejci, D. and Seifert, B., *Propulsion for nanosatellites*, in 32nd International Electric Propulsion Conference, Wiesbaden, Germany, IEPC-2011 (Vol. 171), 2011.

[34] Komurasaki and Koizumi Lab., Department of Aeronautics and Astronautics, The University of Tokyo, found in: http://www.al.t.u-tokyo.ac.jp/ppt_e.html.

[35] Kh.I. Khalil and S.W. Samwel, *Effect of Air Drag Force on Low Earth Orbit Satellites During Maximum and Minimum Solar Activity*, Space Res. J., 9: 1-9, 2016.

[36] Wekerle, T., Pessoa Filho, J. B., Costa, L. E. V. L. D. and Trabasso, L. G., *Status and trends of smallsats and their launch vehicles—An up-to-date review*, Journal of Aerospace Technology and Management, 9(3), 269-286, 2017.

[37] Wang, Y., Ding, W., Cheng, L., Yan, J., Li, Z., Wang, J. and Wang, Y., *An Investigation of Discharge Characteristics of an Electrothermal Pulsed Plasma Thruster*, IEEE Transactions on Plasma Science, 45(10), 2715-2724, 2017.

[38] David Darling, found in: http://www.daviddarling.info/encyclopedia/A/arcjet.html, 2016.

[39] Wilson, M. J., Bushman, S. S. and Burton, R. L., *A compact thrust stand for pulsed plasma thrusters*, IEPC Paper, (97-122), 1997.

[40] Turchi, P., Mikellides, I., Mikellides, P. and Schmahl, C., *Theoretical investigation of pulsed plasma thrusters*, in 34th AIAA/ASME/SAE/ASEE Joint Propulsion Conference and Exhibit (p. 3807), 1998.